AD-A245 553

AN EFFICIENT HYBRID GTD-MODAL
ANALYSIS OF THE SCATTERING
BY AN OPEN-ENDED DIELECTRIC FILLED
CAVITY IN A GROUND PLANE

by

M. C. Liang, P. H. Pathak and C. W. Chuang

The Ohio State University

ElectroScience Laboratory

Department of Electrical Engineering
Columbus, Ohio 43212

92 2 06 064

92-03075

NOTICES

When Government drawings, specifications, or other data are used for any purpose other than in connection with a definitely related Government procurement operation, the United States Government thereby incurs no responsibility nor any obligation whatsoever, and the fact that the Government may have formulated, furnished, or in any way supplied the said drawings, specifications, or other data, is not to be regarded by implication or otherwise as in any manner licensing the holder or any other person or corporation, or conveying any rights or permission to manufacture, use, or sell any patented invention that may in any way be related thereto.

50272-101

REPORT DOCUMENTATION PAGE	1. REPORT NO.	2.	3. Recipient s Accession No

4. Title and Subtitle	5. Report Date
AN EFFICIENT HYBRID GTD-MODAL ANALYSIS OF THE SCATTERING BY AN OPEN-ENDED DIELECTRIC FILLED CAVITY IN A GROUND PLANE	July 1987
	6.

7. Author(s)	8. Performing Organization Rept. No
M.C. Liang, P.H. Pathak, C.W. Chuang	716611-2

9. Performing Organization Name and Address	10. Project/Task/Work Unit No
The Ohio State University ElectroScience Laboratory 1320 Kinnear Road Columbus, Ohio 43212	
	11. Contract(C) or Grant(G) No
	(C) F33615-84-K-1550
	(G)

12. Sponsoring Organization Name and Address	13. Type of Report & Period Covered
USAF/AFSC Aeronautical Systems Division Wright-Patterson AFB, OH 45433	Technical
	14.

15. Supplementary Notes

16. Abstract (Limit 200 words)

The problem of electromagnetic scattering by an open-ended dielectric filled 2-D rectangular cavity in a ground plane is analyzed in an efficient manner via a hybrid combination of ray and modal techniques. In this analysis, the generalized scattering matrices for the junctions pertaining to the discontinuities at the open front end and the back termination are found in a conceptually simple fashion via the geometrical theory of diffraction (GTD) and its modifications, rather than via the conventional and more cumbersome modal matching procedure. The relatively simple expressions obtained for the elements of the scattering matrices essentially describe the complex modal amplitudes of the waves reflected and transmitted by the junctions. The multiple interactions of the modal waves between the junctions are easily accounted for via the generalized scattering matrix technique. The solution explicitly contains the contributions to the scattered field which are due to the diffraction from the open end and the interior cavity effects. These concepts are illustrated only for the two-dimensional case here. However, this hybrid scheme can be readily extended to treat three-dimensional separable cavity configurations. Numerical results based on this hybrid solution are shown to agree well with those based on an independent moment method solution.

17. Document Analysis   a. Descriptors

b. Identifiers/Open-Ended Terms

c. COSATI Field/Group

18. Availability Statement	19. Security Class (This Report)	21. No of Pages
Approved for public release; distribution is unlimited.	Unclassified	64
	20. Security Class (This Page)	22. Price
	Unclassified	

Contents

iii

List of Figures

I Introduction

A hybrid combination of the geometrical theory of diffraction (GTD) [1] -[4] and modal methods are employed within the framework of the generalized scattering matrix technique (GSMT) [5] to efficiently analyze the electromagnetic scattering by an open-ended, dielectric filled rectangular cavity in a perfectly conducting ground plane where the medium external to the cavity is assumed to be free space. This analysis is described here for the two dimensional (2-D) cavity of Figure 1 in free space which is excited by either a TE_z or TM_z plane wave; however, the concepts involved can be readily extended to treat three dimensional rectangular, circular or other separable cavity configurations by augmenting the GTD with other asymptotic high frequency methods as shown in [6]. An analysis of the latter three dimensional (3-D) case will be reported separately. Even though the width of the cavity is shown to be much larger than its depth in Figure 1, this is not a restriction in the present analysis which can also accommodate cavity depths that are larger than its width.

In this hybrid analysis, the elements of the generalized scattering matrices associated with the junctions at the open front end and the back termination are found in a conceptually simple manner via high frequency techniques based on the GTD and the equivalent current method (ECM) [7,8]. It is noted here that the ECM employs the GTD to calculate the strengths of the equivalent currents. It is further noted that the high frequency techniques can be used because each waveguide cavity mode can be

1

decomposed into a set of modal rays [9]. The interaction of these waveguide modes with the discontinuitues, such as the open end, of the cavity can then be analyzed via GTD and ECM by using the diffraction or launching of the corresponding modal rays. The elements of the scattering matrices furnish the complex amplitudes of the waveguide cavity modes which are reflected and transmitted by the junctions. The multiple interactions of the modal waves between the junctions are fully accounted for by the self-consistent multiple scattering approach which is essentially contained in the GSMT. It is important to note that the expressions for the scattering matrices obtained via the GTD are in a relatively simple form; it is for this reason that the present hybrid approach is very efficient. In contrast, the use of conventional mode matching procedures to analyze this problem would be far more cumbersome. Also, the present hybrid method of solution is also far more efficient than a moment method solution of this problem. On the other hand, the present analysis is approximate because GTD is an asymptotic method; however, it is also quite accurate as the numerical results based on this approach are shown to agree well with those based on an independent moment method solution for this problem. At the present time, the directions of incidence and scattering are restricted to about 10° away from grazing with respect to the ground plane; further study to remove this restriction will be pursued in the future.

The format of this paper is as follows. First a self-consistent formulation of the GSMT is presented in section II. This self-consistent approach [10] for summing the multiple wave interactions between the junctions formed

by the open front end and the back termination, respectively, is slightly different from the Neumann series summation approach used in the original development of the GSMT [5]; however, it leads to the same result for the multiple interactions as in the original GSMT. The various junction scattering matrices are also defined in section II. In section III, the GTD and ECM are employed to calculate the elements of the junction scattering matrices. The scattering matrices are combined in section IV according to the expressions for the multiple wave interaction of section II to obtain numerical results for the fields scattered by the cavity when it is illuminated by a plane wave. Numerical results are presented for the backscattering as well as for the bistatic scattering from the cavity shown in Figure 1. An $e^{j\omega t}$ time convention is assumed and suppressed throughout this analysis.

II   Self-Consistent Formulation of the GSMT

In the GSMT [5], the basic scattering mechanisms for the configuration in Figure 1 can be isolated and identified as being associated with the junctions formed at the open front end and the back termination, respectively. At the present time the GTD edge diffraction coefficients are available for a conducting wedge; however, the edges at the open end in Figure 1 are also in contact with the dielectric which fills the cavity. Thus, an additional junction is artificially introduced in the analysis so that the GTD for a conducting wedge can be used; this artificial junction can be formed by recessing the dielectric by a small distance δ inside the cavity as shown in

3

Figure 2. An analysis of the problems in Figure 2 leads to a solution for the scattered field of the problem in Figure 1 as $\delta \to 0$; such a technique of introducing a δ which is then allowed to become vanishingly small has been employed successfully in the past to analyze many scattering problems via the GSMT [5,11]. Three junctions are now identified at the discontinuities as shown in Figure 2; these junctions are labeled I, II and III, respectively.

The scattering matrices associated with the junctions I, II and III describe the isolated scattering events at these junctions as shown in Figure 3. The GSMT extends the concept of the conventional scattering matrix for propagating waveguide modes to include evanescent modes, and it also includes the exterior scattering matrix. The various scattering matrices associated with junctions I and II are shown below; it is noted that in this special case, the effect of junction III is combined into the scattering matrix characterizing junction II and is hence not treated separately.

The multiple scattering between the junctions is calculated via a self-consistent procedure which requires a knowledge of the generalized scattering matrices $[S_{11}]$, $[S_{12}]$, $[S_{21}]$, $[S_{22}]$, and $[S_{\Gamma}]$ for the junctions I and II.

Let $\bar{E}^i$ denote the electric field of the incident electromagnetic plane wave. The electric field contains only the $\hat{z}$ component for the TM_z case and it contains only the $\hat{\theta}$ component for the TE_z case. Thus, one may express $\bar{E}^i$ in general as:

$$\bar{E}^i = E_z^i \hat{z} + E_\theta^i (-\hat{\theta}^i) \tag{1}$$

4

with

$$E_z^i = A_z e^{-j\bar{k}^i \cdot \bar{\rho}};\tag{2}$$

$$E_\theta^i = A_\theta e^{-j\bar{k}^i \cdot \bar{\rho}};\tag{3}$$

where

$$\bar{k}^i = -k_o(\cos\theta^i \hat{x} + \sin\theta^i \hat{y}),\tag{4}$$

and

$$\bar{\rho} = x\hat{x} + y\hat{y}.\tag{5}$$

It is noted that k_o refers to the free space wavenumber and $\bar{\rho}$ is the position vector of the observation point P. The unit vector $\hat{\theta}^i$ is shown in Figure 1.

The matrix $[S_{11}]$ relates the scattered electric field $\bar{E}^{so}$ from only the open end at $x = 0$ to the field $\bar{E}^i$ which is incident at the open end. One may then describe the scattering matrix $[S_{11}]$ as follows:

$$\begin{bmatrix} E_z^{so} \\ E_\theta^{so} \end{bmatrix} = \begin{bmatrix} S_{zz}^{so} & S_{z\theta}^{so} \\ S_{\theta z}^{so} & S_{\theta\theta}^{so} \end{bmatrix} \begin{bmatrix} A_z \\ A_\theta \end{bmatrix}\tag{6}$$

where

$$\bar{E}^{so} = E_z^{so}\hat{z} + E_\theta^{so}\hat{\theta}\tag{7}$$

5

and the unit vector $\hat{\theta}$ is also shown in Figure 1. From (6),

$$[S_{11}] = \left[\begin{array}{cc} S_{zz}^{so} & S_{z\theta}^{so} \\ S_{\theta z}^{so} & S_{\theta\theta}^{so} \end{array} \right] \tag{8}$$

The scattering matrix $[S_{12}]$ converts the waveguide modal fields incident at the open end ($x = 0$) from the interior region to the field radiated by these modes from the open end as shown in Figure 3(b). The modal electric field $\bar{E}_g^{\pm}$ within the waveguide portion of the cavity may be represented as

$$\bar{E}_g^{\pm} = \sum_{n=0}^{\infty} \left(A_n^{\pm} e_z \hat{z} + B_n^{\pm} \bar{e}_t \right) e^{\mp j\beta_n x} \tag{9}$$

The terms $A_n^{\pm}$ and $B_n^{\pm}$ are the amplitudes of the modal fields in the waveguide section. The $\bar{e}_t$ denotes the nth modal electric field in the TE_z case for which the magnetic field had only a $\hat{z}$-component. Likewise, $e_z \hat{z}$ denotes the nth modal electric field which is entirely in the $\hat{z}$-direction for the TM_z case. The propagation constants β_n for the nth mode are the same for the TE_z and TM_z cases. Also note that $n > 0$ for the TM_z case. The superscripts $+$ and $-$ in (9) refer to modes propagating in the $+\hat{x}$ and $-\hat{x}$ directions, respectively. These waveguide modes are defined in detail in Appendix A. If $\bar{E}^{ro}$ denotes the electric field at P exterior to the cavity due to the radiation of the modes that impinge on the open end, then the scattering matrix $[S_{12}]$ relates $\bar{E}^{ro}$ to $\bar{E}_g^{+}$ as follows:

6

$$
\begin{bmatrix} E_z^{ro} \\ E_\theta^{ro} \end{bmatrix} = \begin{bmatrix} \begin{bmatrix} S_{zA_n}^{ro} \end{bmatrix} & \begin{bmatrix} S_{zB_n}^{ro} \end{bmatrix} \\ \begin{bmatrix} S_{\theta A_n}^{ro} \end{bmatrix} & \begin{bmatrix} S_{\theta B_n}^{ro} \end{bmatrix} \end{bmatrix} \begin{bmatrix} [A_n^+] \\ [B_n^+] \end{bmatrix} \frac{e^{-jk\rho}}{\sqrt{\rho}} \tag{10}
$$

where

$$
[S_{12}] = \begin{bmatrix} \begin{bmatrix} S_{zA_n}^{ro} \end{bmatrix} & \begin{bmatrix} S_{zB_n}^{ro} \end{bmatrix} \\ \begin{bmatrix} S_{\theta A_n}^{ro} \end{bmatrix} & \begin{bmatrix} S_{\theta B_n}^{ro} \end{bmatrix} \end{bmatrix} \tag{11}
$$

Notice that each of the submatrices in (11) separately contain the $\hat{z}$ and $\hat{\theta}$ components of the fields radiated by each of the TM_z modes and the TE_z modes respectively. For example, each element of $\begin{bmatrix} S_{zA_n}^{ro} \end{bmatrix}$ gives the $\hat{z}$ component of the electric field radiated by each of the TM_z mode of amplitude A_n^+. Therefore, if the total numbers of the TM_z and TE_z modes included in the calculation are N_h and N_e, respectively. The order of the submatrices $\begin{bmatrix} S_{zA_n}^{ro} \end{bmatrix}$, $\begin{bmatrix} S_{\theta A_n}^{ro} \end{bmatrix}$, $\begin{bmatrix} S_{zB_n}^{ro} \end{bmatrix}$, $\begin{bmatrix} S_{\theta B_n}^{ro} \end{bmatrix}$, $[A_n^+]$, and $[B_n^+]$ will be $1 \times N_h$, $1 \times N_h$, $1 \times N_e$, $1 \times N_e$, $N_h \times 1$, and $N_e \times 1$, respectively.

Similarly, the scattering matrix $[S_{21}]$ describes the coupling of the incident plane wave field into the waveguide modes as shown in Figure 3(b). Therefore, $[S_{21}]$ relates $\bar{E}_g^-$ to $\bar{E}^i$ as follows:

$$
\begin{bmatrix} [A_n^-] \\ [B_n^-] \end{bmatrix} = \begin{bmatrix} \begin{bmatrix} S_{A_n z}^c \end{bmatrix} & \begin{bmatrix} S_{A_n \theta}^c \end{bmatrix} \\ \begin{bmatrix} S_{B_n z}^c \end{bmatrix} & \begin{bmatrix} S_{B_n \theta}^c \end{bmatrix} \end{bmatrix} \begin{bmatrix} A_z \\ A_\theta \end{bmatrix} \tag{12}
$$

where

7

$$[S_{21}] = \left[\begin{array}{cc} \left[S^c_{A_n z}\right] & \left[S^c_{A_n \theta}\right] \\ \left[S^c_{B_n z}\right] & \left[S^c_{B_n \theta}\right] \end{array} \right] \tag{13}$$

Again, the order of the submatrices $\left[S^c_{A_n z}\right]$, $\left[S^c_{A_n \theta}\right]$, $\left[S^c_{B_n z}\right]$, $\left[S^c_{B_n \theta}\right]$, $[A_n^-]$, and $[B_n^-]$ are $N_h \times 1$, $N_h \times 1$, $N_e \times 1$, $N_e \times 1$, $N_h \times 1$, and $N_e \times 1$, respectively. It is noted that the problem of determining the matrix $[S_{12}]$ is related to that of $[S_{21}]$ by reciprocity. The explicit relationship is given in the next section.

The scattering matrix $[S_{22}]$ is the modal reflection coefficient associated with the interaction at the open end of the waveguide which relates the amplitude (A_n^- or B_n^-) of the nth (TM$_z$ or TE$_z$) mode which is reflected from the open end when a qth (TM$_z$ or TE$_z$) mode of amplitude (A_q^+ or B_q^+) is incident at the open end. Thus,

$$\left[\begin{array}{c} [A_n^-] \\ [B_n^-] \end{array} \right] = \left[\begin{array}{cc} \left[R^{hh}_{n;q}\right] & \left[R^{he}_{n;q}\right] \\ \left[R^{eh}_{n;q}\right] & \left[R^{ee}_{n;q}\right] \end{array} \right] \left[\begin{array}{c} [A_q^+] \\ [B_q^+] \end{array} \right] \tag{14}$$

where

$$[S_{22}] = \left[\begin{array}{cc} \left[R^{hh}_{n;q}\right] & \left[R^{he}_{n;q}\right] \\ \left[R^{eh}_{n;q}\right] & \left[R^{ee}_{n;q}\right] \end{array} \right] \tag{15}$$

Also, notice that the submatrices $\left[R^{hh}_{n;q}\right]$, $\left[R^{he}_{n;q}\right]$, $\left[R^{eh}_{n;q}\right]$, and $\left[R^{ee}_{n;q}\right]$ are of order $N_h \times N_h$, $N_h \times N_e$, $N_e \times N_h$, and $N_e \times N_e$, respectively.

8

The scattering matrix $[S_\Gamma]$ is the modal reflection coefficient associated with the termination at junction II which relates the coefficients or amplitudes of the waveguide modes $\bar{E}_q^-$ incident on the termination to the coefficients of the waveguide modes $\bar{E}_n^+$ reflected from that termination. Thus,

$$\left[\begin{array}{c} [A_n^+] \\ [B_n^+] \end{array}\right] = \left[\begin{array}{cc} \left[\Gamma_{n;q}^{hh}\right] & \left[\Gamma_{n;q}^{he}\right] \\ \left[\Gamma_{n;q}^{eh}\right] & \left[\Gamma_{n;q}^{ee}\right] \end{array}\right] \left[\begin{array}{c} [A_q^-] \\ [B_q^-] \end{array}\right] \tag{16}$$

where

$$[S_\Gamma] = \left[\begin{array}{cc} \left[\Gamma_{n;q}^{hh}\right] & \left[\Gamma_{n;q}^{he}\right] \\ \left[\Gamma_{n;q}^{eh}\right] & \left[\Gamma_{n;q}^{ee}\right] \end{array}\right] \tag{17}$$

Again, the submatrices $\left[\Gamma_{n;q}^{ee}\right]$, $\left[\Gamma_{n;q}^{ee}\right]$, $\left[\Gamma_{n;q}^{ee}\right]$, and $\left[\Gamma_{n;q}^{ee}\right]$ are of order $N_h \times N_h$, $N_h \times N_e$, $N_e \times N_h$, and $N_e \times N_e$, respectively.

At any given frequency, the waveguide can support a finite number of propagating modes and an infinite number of evanescent modes. However, due to reasons similar to those discussed in [9], only a finite number of evanescent modes will contribute significantly to the radiation problem as $\delta \to 0$, so that only a finite number of evanescent modes needs to be included in practice.

It is observed from Figure 4 that one may describe the field scattered by the cavity as consisting of two parts. The entire scattered field thus consists of the contribution from just the open end by itself, together with

9

the field radiated from the open end as a result of all the interactions between the open end and the termination that arise from the incident field which is coupled into the waveguide cavity region. Referring to Figure 4, it is observed that the incident electric field $\bar{E}^i$ at the open end is partly scattered by junction I to produce a scattered field $\bar{E}^{so}$ given by (6) and (8). The rest of the incident field is also coupled at I into the waveguide region provided that there is no other scattering from the external part of the cavity; this field then becomes incident at junction II from which it is subsequently reflected. The field reflected from junction II is incident back at I where it undergoes further scattering into the exterior and interior regions, and so on, thus giving rise to multiple wave interactions between junctions I and II. The fields resulting from these multiple interactions may be expressed in a convergent Neumann series as done by *Pace and Mittra* [11]; however, an alternate procedure based on a self-consistent method [10] leads directly to the same result. The latter self-consistent MSM based analysis will be employed here.

Let $[E_{12}]$ represent the total field incident at I from II after taking all the multiple interactions into account. Likewise, let $[E_{21}]$ represent the total field incident at II from I after taking all the multiple interactions into consideration. Then the total scattered field in the exterior region denoted by $[E^s]$ consists of a superposition of $[E^{so}]$ and $[E^{mo}]$, where $[E^{mo}]$ is the field scattered into the exterior region when $[E_{12}]$ is incident on I. Therefore,

10

$$[E^s] \;=\; [E^{so}] + [E^{mo}] \tag{18}$$

where $[E^{mo}]$ may be expressed as

$$[E^{mo}] \;=\; [S_{12}][E_{12}]\big|_{z=0} . \tag{19}$$

The expressions for [E_{12}] and [E_{21}] may be written in terms of the matrices defined above; namely,

$$[E_{21}]\big|_{z=0} = \Big\{ [S_{21}][E^i] + [S_{22}][E_{12}] \Big\}\Big|_{z=0} \tag{20}$$

and

$$[E_{12}]\big|_{z=0} \;=\; [P][S_{\Gamma}][P][E_{21}]\big|_{z=0} \tag{21}$$

in which $[S_{\Gamma}]$ denotes the reflection coefficient scattering matrix pertaining to junction II as defined in (17), and [P] is a diagonal matrix accounting for the phase path delay along the length L between junctions I and II. Eliminating $[E_{12}]$ between (20) and (21) yields

$$([I] - [S_{22}][P][S_{\Gamma}][P]) \, [E_{21}]\big|_{z=0} = [S_{21}][E^i], \tag{22}$$

where [I] is an identity matrix. Hence, it follows that

11

$$[E_{21}]|_{z=0} = ([I] - [S_{22}][P][S_\Gamma][P])^{-1} [S_{21}][E^i]. \qquad (23)$$

From (21), $E_{12}|_{z=0}$ becomes

$$[E_{12}]|_{z=0} = [P][S_\Gamma][P] ([I] - [S_{22}][P][S_\Gamma][P])^{-1} [S_{21}][E^i]. \qquad (24)$$

Incorporating the above result into (19) yields

$$[E^{mo}] = [S_{12}][P][S_\Gamma][P] ([I] - [S_{22}][P][S_\Gamma][P])^{-1} [S_{21}][E^i]. \qquad (25)$$

Finally, combining (6) and (19) according to (18) leads to the self-consistent expression for the total scattered field $[E^s]$ as

$$[E^s] = \{[S_{11}] + [S_{12}][P][S_\Gamma][P] ([I] - [S_{22}][P][S_\Gamma][P])^{-1} [S_{21}]\}[E^i]. \ (26)$$

The scattering matrices $[S_{11}], [S_{12}], [S_{21}]$, and $[S_{22}]$ can be found in a relatively simple manner via the GTD and ECM as shown in the next section.

III Analysis for Determining the Elements of the Scattering Matrices

The elements of $[S_{11}]$ can be found via a direct application of GTD which provides the fields diffracted from the edges at the open end of the cavity

when a plane wave is incident on these edges. Using the concept of modal rays one can also find the elements of $[S_{12}]$ directly using the GTD. On the other hand, it is necessary to employ GTD based ECM to find the elements of $[S_{21}]$ and $[S_{22}]$; however, $[S_{21}]$ is related to $[S_{12}]$ via reciprocity and it can therefore be found by invoking reciprocity once $[S_{12}]$ is known.

For the dielectric loaded cavity considered in this report, the contribution to the scattered field arising from the multiple wave interactions between edges is significant outside the specular direction. Therefore, the field doubly diffracted across the open end is also included in the $[S_{11}]$, $[S_{12}]$, $[S_{22}]$ calculation of the scattered field.

It has also been found that when the incident angle is away from grazing the ground plane, a simple formulation for the doubly diffracted field across the open end can be calculated by the equivalent current method. However, at and near grazing incidence, this simple formulation for the doubly diffracted field is no longer valid. In this case, a more elaborate formula by Tiberio and Kouyoumjian [12] (TK) as shown in Appendix B has to be used for calculating the doubly diffracted field. The TK doubly diffracted field properly compensates the singularity of the singly diffracted field. However, the TK formulation is much more complicated which results in a much longer computation time and the results are essentially the same as those obtained from the simple formulation mentioned above when the incident angle is away from grazing the ground plane. It is for this reason that the doubly diffracted field in this report is given in terms of the simple GTD formulation, and for near grazing incidence these doubly diffracted

13

fields can be replaced by the TK formulation as in Appendix B.

It is noted that with the TK formulation, the singularity in the singly diffracted field at grazing incidence can been properly corrected. But the singularity in the doubly diffracted field still remains. This additional singularity in the doubly diffracted field can again be corrected by including higher order (triply, quadruply, $\cdots$) diffracted fields. But then, the computation will become too cumbersome to be useful for practical purposes. To avoid the need of including the triply and higher order diffracted fields, a cosine factor is introduced into the doubly diffracted field in the exterior region. This cosine factor forces the doubly diffracted fields to vanish along the part of the ground plane where the doubly diffracted fields alone do not satisfy the boundary conditions. Specifically, this is done as follows: Divide *the exterior free space into two quadrants.* Each doubly diffracted ray will properly pair up with the singly diffracted ray and therefore no modification is needed in one of the quadrants that encloses the edge where the doubly diffracted ray emanates. In the other quadrant, the doubly diffracted ray becomes singular at grazing incidence without proper compensation and so a cosine factor $\cos\theta$, $0 \leq \theta \leq \pi/2$, is included, where $\theta = 0°$ is chosen to be the boundary between the two quadrants and the modification factor is one at the boundary and zero in the singular direction.

In addition, it is also found that evanescent modes with a high reflection coefficient $[S_\Gamma]$ also contribute significantly to the scattered field outside the specular region and therefore they must be included in the calculation. From the cases treated here, it is found that generally only the first 5 or 6

evanescent modes are needed for accuracy. In order to account for the effect of the evanescent modes by using the GTD and ECM, it has been necessary to generalize Keller's edge diffraction coefficient $D_{s,h}$ (see Equation (29) below) to include complex angles of incidence and diffraction.

III.1 Development of $[S_{11}]$

The matrix $[S_{11}]$ describes the field scattered only from the open end of the cavity. The elements of $[S_{11}]$ can be found via the GTD as indicated earlier. Since there is no coupling between the $\hat{z}$ and $\hat{\theta}$ polarizations for the 2-D case, the off-diagonal elements $S_{z\theta}^{so}$ and $S_{\theta z}^{so}$ in $[S_{11}]$ vanish. The diagonal elements S_{zz}^{so} and $S_{\theta\theta}^{so}$ can be found via GTD as follows:

The field $\bar{E}^{so}$ scattered from just the open end is given by

$$\bar{E}^{so} = \bar{E}_1^{so} + \bar{E}_2^{so} \tag{27}$$

where $\bar{E}_{1,2}^{so}$ are the fields diffracted from the top / bottom edge at $x = \pm a/2$. The $\bar{E}_1^{so}$ and $\bar{E}_2^{so}$ are given in terms of the GTD by

$$\bar{E}_{1,2}^{so} \sim \bar{E}^i(Q_{1,2}) \cdot \overline{\overline{D}} \frac{e^{-jks_{1,2}}}{\sqrt{s_{1,2}}} + \bar{E}^i(Q_{1,2}) \cdot \overline{\overline{D}}_d \frac{e^{-jks_{2,1}}}{\sqrt{s_{2,1}}} \; ; \tag{28}$$

where $\overline{\overline{D}}$ is the dyadic form of the 2-D version of Keller's diffraction coefficient, which is given by

$$\overline{\overline{D}} \;=\; D_s(\phi', \phi, n)\hat{z}\hat{z} - D_h(\phi', \phi, n)\hat{\theta}_i\hat{\theta}_s$$

15

and $\overline{\overline{D}}_d$ is the dyadic form of the 2-D version of the double diffraction coefficient. For incident angle away from grazing angle of the ground plane, a simple double diffraction coefficient based on the equivalent current method can be applied and one finds that

$$\overline{\overline{D}}_d = D_s(\phi', \phi_{12}, n)D_s^{U}(L, \phi_{12}, \phi, n)\hat{z}\hat{z} \tag{29}$$
$$-D_h(\phi', \phi_{12}, n)D_h^{U}(L, \phi_{12}, \phi, n)\hat{\theta}_i\hat{\theta}_s$$

where ϕ_{12} is the angle of the singly diffracted ray incident from edge 1 to edge 2 and $D_{s,h}^{U}$ represent the UTD [3] diffraction coefficients. Then from (6) it is clear that:

$$
\begin{aligned}
S_{zz}^{so} =\ & e^{jk_o \frac{a}{2}(\sin\theta_i + \sin\theta_s)}D_s(\pi + \theta_i, \pi + \theta_s) \\
& + e^{-jk_o \frac{a}{2}(\sin\theta_i + \sin\theta_s)}D_s(\pi - \theta_i, \pi - \theta_s) \\
& + \frac{e^{jk_o \frac{a}{2}(\sin\theta_i - \sin\theta_s) - jk_o a}}{\sqrt{a}}D_s(\pi + \theta_i, \frac{\pi}{2})D_s^{U}(k_o a, \frac{\pi}{2}, \pi - \theta_s) \\
& + \frac{e^{jk_o \frac{a}{2}(\sin\theta_s - \sin\theta_i) - jk_o a}}{\sqrt{a}}D_s(\pi - \theta_i, \frac{\pi}{2})D_s^{U}(k_o a, \frac{\pi}{2}, \pi + \theta_s) \quad (30)
\end{aligned}
$$
$$
\begin{aligned}
S_{\theta\theta}^{so} =\ & e^{jk_o \frac{a}{2}(\sin\theta_i + \sin\theta_s)}D_h(\pi + \theta_i, \pi + \theta_s) \\
& + e^{-jk_o \frac{a}{2}(\sin\theta_i + \sin\theta_s)}D_h(\pi - \theta_i, \pi - \theta_s) \\
& + \frac{e^{jk_o \frac{a}{2}(\sin\theta_i - \sin\theta_s) - jk_o a}}{\sqrt{a}}D_h(\pi + \theta_i, \frac{\pi}{2})D_h^{U}(k_o a, \frac{\pi}{2}, \pi - \theta_s) \\
& + \frac{e^{jk_o \frac{a}{2}(\sin\theta_s - \sin\theta_i) - jk_o a}}{\sqrt{a}}D_h(\pi - \theta_i, \frac{\pi}{2})D_h^{U}(k_o a, \frac{\pi}{2}, \pi + \theta_s). \quad (31)
\end{aligned}
$$

The first two terms in Equations (30) and (31) are the fields associated with rays singly diffracted from each of the two edges at the open end;

16

whereas, the third and fourth terms are the fields associated with rays that are doubly diffracted from those edges. The doubly diffracted field is produced when the singly diffracted field from one edge is incident at the opposite edge. The $D_{s,h}(\phi',\phi)$ in (30) and (31) represent Keller's GTD edge diffraction coefficients [1] with $n = 3/2$; the $D_{s,h}$ are valid only outside the shadow boundary transition regions. The $D_{s,h}^{U}(L,\phi',\phi)$ represent the uniform GTD (UTD) edge diffraction coefficients [3] with $n = 3/2$. It is noted that the $D_{s,h}^{U}$ remain valid within the shadow boundary transition regions and reduce to $D_{s,h}$ outside those regions [3].

III.2 Development of $[S_{12}]$

The radiation matrix $[S_{12}]$ describes the radiation of the waveguide cavity modes from the open end into the external free space. The elements of this matrix are found through the use of the GTD; here, the idea is to decompose the waveguide modes incident at the open end into modal rays. Each modal ray is treated as a plane wave incident on the appropriate edge from the modal ray direction which is diffracted from the edge into the exterior region as shown in Figure 5. The radiated electric field has only a $\hat{z}$-component for the TM$_z$ modes and only a $\hat{\theta}$-component for the TE$_z$ modes. Therefore, $S_{zB_n}^{ro}$ and $S_{\theta A_n}^{ro}$ are zero; and the elements $S_{zA_n}^{ro}$ and $S_{\theta B_n}^{ro}$ can be found to be

$$S_{zA_n}^{ro} = -j\sqrt{\frac{k_0 Z_0}{2\beta_n a}}\left[(-1)^{n+1}e^{jk_0\frac{a}{2}\sin(\theta_s)}D_s(\delta_n,\pi+\theta_s)\right.$$

17

$$+ e^{-jk_o \frac{a}{2} \sin(\theta_s)} D_s(\delta_n, \pi - \theta_s)$$

$$+ (-1)^{n+1} e^{-jk_o \frac{a}{2} \sin(\theta_s)} D_s(\delta_n, \frac{\pi}{2}) \frac{e^{-jka}}{\sqrt{a}} D_s^U(k_o a, \frac{\pi}{2}, \pi - \theta_s)$$

$$+ e^{jk_o \frac{a}{2} \sin(\theta_s)} D_s(\delta_n, \frac{\pi}{2}) \frac{e^{-jka}}{\sqrt{a}} D_s^U(k_o a, \frac{\pi}{2}, \pi + \theta_s) \Bigg] \qquad (32)$$

$$S_{\theta B_n}^{ro} = \sqrt{\frac{k_o Z_o}{2\epsilon_{n0}\beta_n a}} \Bigg[(-1)^n e^{jk_o \frac{a}{2} \sin(\theta_s)} D_h(\delta_n, \pi + \theta_s)$$

$$+ e^{-jk_o \frac{a}{2} \sin(\theta_s)} D_h(\delta_n, \pi - \theta_s)$$

$$+ (-1)^n e^{-jk_o \frac{a}{2} \sin(\theta_s)} D_h(\delta_n, \frac{\pi}{2}) \frac{e^{-jka}}{\sqrt{a}} D_h^U(k_o a, \frac{\pi}{2}, \pi - \theta_s)$$

$$+ e^{jk_o \frac{a}{2} \sin(\theta_s)} D_h(\delta_n, \frac{\pi}{2}) \frac{e^{-jka}}{\sqrt{a}} D_h^U(k_o a, \frac{\pi}{2}, \pi + \theta_s) \Bigg] \qquad (33)$$

where

$$\delta_n = \sin^{-1}\left(\frac{n\pi}{ka}\right). \qquad (34)$$

It is noted that the effect of rays doubly diffracted from the edges is included in the above expressions.

III.3   Reciprocity Relationship between $[S_{12}]$ and $[S_{21}]$

As discussed in the previous section, the elements of the matrix $[S_{12}]$ can be related to that of $[S_{21}]$ by reciprocity [13]. For the 2-D problem discussed here, the relationship becomes

$$[S_{21}] = \frac{1}{Z_o} \sqrt{\frac{2\pi}{jk}} [S_{12}]^T. \qquad (35)$$

III.4   Development of $[S_{22}]$

The elements of $[S_{22}]$ are the modal reflection coefficients of the nth mode reflected from the open end due to a qth mode incident on the open end.

18

These modal reflection coefficients for the open end can be found through the help of the ECM [6] in which the strengths of the equivalent currents are found from the GTD. In order to apply the GTD and ECM methods, an incident waveguide mode is first decomposed into a pair of bouncing modal rays for the parallel plate waveguide [9]. Each modal ray can be treated as a plane wave which is incident on the edge in the direction of the modal ray angle as in Figure 5. Only one set of modal rays is incident on an edge to produce diffracted rays. The effect of the field doubly diffracted between the edges is included by treating the singly diffracted field from one edge as being the field incident on the second edge to produce the doubly diffracted field. The edge diffracted fields can be found in terms of the GTD edge diffraction coefficients $D_{s,h}$; these diffracted fields can be viewed as being produced by a pair of equivalent line currents at the two edges. The equivalent currents can be chosen to radiate inside the semi-infinite waveguide (and its geometric extension to form an infinite waveguide); the amplitudes of the modal fields excited by these equivalent currents within the original semi-infinite portion of the waveguide then constitute the required modal reflection coefficients as shown in [14]. For propagating modes, $n\pi < ka$ so the modal angle $\delta_n = \sin^{-1}(\frac{n\pi}{ka})$ as shown in Figure 5 is real. For evanescent modes, $n\pi > ka$ so the modal angle is pure imaginary. As a result of the orthogonality property of the waveguide modes, the elements $R_{n;q}^{he}$ and $R_{n;q}^{eh}$ can be shown to vanish, and the elements $R_{n;q}^{hh}$ and $R_{n;q}^{ee}$ are given by [9]

19

$$R_{n;q}^{hh} = -\sqrt{\frac{\pi k}{2ja^2\epsilon_{n0}\epsilon_{q0}\beta_n\beta_q}}[(-1)^{q+n}+1]$$

$$\left[D_s(\delta_n,\delta_q) - (-1)^n D_s(\delta_n,\frac{\pi}{2})D_s(\frac{\pi}{2},\delta_q)\frac{e^{-jka}}{\sqrt{a}}\right] \tag{36}$$

$$R_{n;q}^{ee} = +\sqrt{\frac{\pi k}{2ja^2\epsilon_{n0}\epsilon_{q0}\beta_n\beta_q}}[(-1)^{q+n}+1]$$

$$\left[D_h(\delta_n,\delta_q) + (-1)^n D_h(\delta_n,\frac{\pi}{2})D_h(\frac{\pi}{2},\delta_q)\frac{e^{-jka}}{\sqrt{a}}\right]. \tag{37}$$

III.5 Development of $[S_\Gamma]$

The reflection coefficient $[S_\Gamma]$ is the modal reflection coefficient associated with the termination. In Figure 4(a) the cross section of the waveguide cavity is uniform and the interior termination is comprised of a planar, uniform dielectric layer which is normal to the waveguide axis and backed by a short circuit. Therefore, from the orthogonality property of the waveguide modes, there is no coupling between the different waveguide modes across the dielectric interface, and at the short circuit. Accordingly, the matrix $[S_\Gamma]$ becomes diagonal for this case. The elements of $[S_\Gamma]$ are trivially obtained by matching the appropriate boundary conditions on the tangential fields at the dielectric interface and the short circuit, respectively, and by invoking the orthogonality of the modes. Thus, it can be shown that:

$$\left.\begin{array}{c}\Gamma_{n;n}^{hh}\\[2mm]\Gamma_{n;n}^{ee}\end{array}\right\} = \frac{R_n^{12}e^{2j\beta_{n2}L_2} + R_n^{23}}{e^{2j\beta_{n2}L_2} + R_n^{12}R_n^{23}} \tag{38}$$

20

where

$$R_n^{12} = \begin{cases} (\mu_2\beta_{n1} - \mu_1\beta_{n2})/(\mu_2\beta_{n1} + \mu_1\beta_{n2}) & \text{for } \Gamma_{n;n}^{hh} \\ (\epsilon_2\beta_{n1} - \epsilon_1\beta_{n2})/(\epsilon_2\beta_{n1} + \epsilon_1\beta_{n2}) & \text{for } \Gamma_{n;n}^{ee} \end{cases} \tag{39}$$

$$R_n^{23} = \begin{cases} -1 & \text{for } \Gamma_{n;n}^{hh} \\ 1 & \text{for } \Gamma_{n;n}^{ee} \end{cases} \tag{40}$$

and

$$\beta_{n1} = \sqrt{k_o^2\epsilon_1\mu_1 - \left(\frac{n\pi}{a}\right)^2} \tag{41}$$

$$\beta_{n2} = \sqrt{k_o^2\epsilon_2\mu_2 - \left(\frac{n\pi}{a}\right)^2}. \tag{42}$$

IV   Numerical Calculations and Discussion

The accuracy of the present hybrid approach for analyzing the scattering from the dielectric filled cavity in a ground plane is tested by comparing the numerical results obtained using this approach with those based on an independent numerical moment method (MM) solution of an integral equation for the same problem. Several numerical results illustrating this comparison are given in Figures 6 through 12. It is seen from these figures that the results for the bistatic scattering from the cavity can be significantly improved for aspects near the ground plane by including the doubly diffracted rays which result from the interaction between the two edges at

21

the open end. The latter comment applies to both types of incident polarization. For near grazing angles of incidence on the cavity, the scattered field becomes less accurate within 15 degrees or so off the ground plane. This inaccuracy is further enhanced for aspects close to the ground plane when the dielectric constant is made extremely large in the TM_z case as is evident from Figure 12. Although the use of the TK double diffraction formulation generally yields better results at near grazing incidence than those obtained with the simple GTD double diffraction formulation, it still does not completely remove the inaccuracy problem at aspects close to the ground plane. Possibly, the triple and other higher order multiple interactions could provide an additional improvement; however, the calculations to include these become more cumbersome and will not be attempted here.

Additional numerical results for the backscattering from the rectangular cavity in the ground plane are also provided in Figures 13-16. The latter calculations are performed for different widths and depths of the cavity, as well as for different dielectric constants of the material filling the cavity. Again, for the aforementioned reasons, the calculations in those figures should remain accurate except to within 15 degrees or so of the ground plane.

In conclusion, an efficient hybrid method combining the high frequency techniques with the modal approach within the framework of the self consistent multiple scattering formulation (i.e. MSM or equivalently GSMT) has been developed to analyze the scattering by two dimensional dielectric filled rectangular cavities in a ground plane. This approach can be extended

22

to treat the scattering by corresponding three dimensional dielectric filled rectangular, circular or other cavity shapes for which the waveguide cavity modes can be found analytically in closed forms. Furthermore, it is also possible to extend this useful hybrid technique to include the effects of antennas placed within such cavities by combining it with the moment method. The latter topics are proposed as part of a future study.

Appendix A

Waveguide Modes

$$\bar{e}_t = \hat{x}e_x + \hat{y}e_y \tag{43}$$

$$\bar{h}_t = \hat{x}h_x + \hat{y}h_y \tag{44}$$

A. Soft Case (i.e., TM_z Case):

$$e_z(x,y) = A_n \sin[\frac{n\pi}{a}(y + \frac{a}{2})]e^{\pm j\beta_n x} \tag{45}$$

$$h_x(x,y) = \frac{jn\pi}{Z_{eq,n}\beta_n a} A_n \cos[\frac{n\pi}{a}(y + \frac{a}{2})]e^{\pm j\beta_n x} \tag{46}$$

$$h_y(x,y) = \pm\frac{1}{Z_{eq,n}} A_n \sin[\frac{n\pi}{a}(y + \frac{a}{2})]e^{\pm j\beta_n x} \tag{47}$$

$$e_x(x,y) = e_y(x,y) = h_z(x,y) = 0.$$

Where

$$A_n = \sqrt{\frac{2kZ}{\beta_n a}}$$

$$Z_{eq,n} = \frac{kZ}{\beta_n}$$

$$\beta_n = \sqrt{k^2 - (\frac{n\pi}{a})^2}.$$

24

B. Hard Case (i.e., TE_z Case):

$$h_z(x,y) = A_n \cos[\frac{n\pi}{a}(y + \frac{a}{2})]e^{\pm j\beta_n x} \tag{48}$$

$$e_x(x,y) = \frac{jZ_{eq,n}n\pi}{\beta_n a}A_n \sin[\frac{n\pi}{a}(y + \frac{a}{2})]e^{\pm j\beta_n x} \tag{49}$$

$$e_y(x,y) = \mp Z_{eq,n}A_n \cos[\frac{n\pi}{a}(y + \frac{a}{2})]e^{\pm j\beta_n x} \tag{50}$$

$$h_x(x,y) = h_y(x,y) = e_z(x,y) = 0.$$

Where

$$A_n = \sqrt{\frac{2k}{\epsilon_{n0}Z\beta_n a}}$$

$$\epsilon_{n0} = \begin{cases} 1 \text{ for n} \neq 0 , \\ 2 \text{ for n} = 0 \end{cases}$$

$$Z_{eq,n} = \frac{\beta_n Z}{k}$$

$$\beta_n = \sqrt{k^2 - (\frac{n\pi}{a})^2}.$$

25

Appendix B

The Uniform GTD Solution for the Doubly Diffracted Field between Two Edges

The Uniform GTD (UTD) solution for the doubly diffracted field between two edges has been found by Tiberio and Kouyoumjian [12] recently. This solution can properly account for the singularity of the singly diffracted field even when the incident angle is near the grazing angle of these two edges, the detail of this solution can be found in [12]. In this appendix, one lists only 2-D version dyadic form of the solution which is given by

$$\overline{\overline{D}}_d(Q_1, Q_2) = \hat{z}\hat{z}D_{ds} - \hat{\phi}_1'\hat{\phi}_2'D_{dh}, \tag{51}$$

where

$$D_{ds,dh} = P_{e,m}(Q_1, Q_2) \tag{52}$$

$$P_{e,m}(Q_1, Q_2) \sim \sum_{p=1}^{4}\sum_{q=1}^{4}\frac{\chi_p\chi_q}{2}[P_s(\Phi_p, \Phi_q) + P_h(\Phi_p, \Phi_q)] \tag{53}$$

$$\cdot \; P_s(\Phi_p, \Phi_q) \sim \frac{(-1)^{p+q}}{8\pi j(n_1 n_2)^2}\frac{a_p a_q}{\sin^2\frac{\Phi_p}{2n_1}\sin^2\frac{\Phi_q}{2n_2}}$$
$$\cdot \frac{F(kLa_p) - F(kLa_q)}{a_p - a_q}\frac{e^{-jka}}{\sqrt{k^2a}} \tag{54}$$

$$P_h(\Phi_p, \Phi_q) \sim \frac{-1}{4\pi j(n_1 n_2)}\cot\frac{\Phi_p}{2n_1}\cot\frac{\Phi_q}{2n_2}$$

$$\cdot \frac{a_q F(kLa_p) - a_p F(kLa_q)}{a_p - a_q} \frac{e^{-jka}}{\sqrt{k^2 a}} \tag{55}$$

$$\Phi_p = \pi + (-1)^p [\phi_1 - \eta_p \phi_1'], \quad p = 1,4 \tag{56}$$

$$\Phi_q = \pi + (-1)^q [\phi_2 - \eta_q \phi_q'], \quad q = 1,4 \tag{57}$$

$$a_p = 2\cos^2[(\Phi_p - \pi - (-1)^p 2n_1 \pi N_p)/2.] \tag{58}$$

$$a_q = 2\cos^2[(\Phi_q - \pi - (-1)^q 2n_2 \pi N_q)/2.] \tag{59}$$

N_p is the integer that most nearly equals$(-1)^p \dfrac{\Phi_p}{2n_1 \pi}$

N_q is the integer that most nearly equals$(-1)^q \dfrac{\Phi_q}{2n_2 \pi}$

$$\eta_i = \begin{cases} 1 \text{ for } i = 1,2 \\ -1 \text{ for } i = 3,4. \end{cases}$$

$$\chi_i = \begin{cases} \eta_i \text{ for } TM_z \text{ case, i.e. } P_e \\ 1 \text{ for } TE_z \text{ case, i.e. } P_m \end{cases}$$

The angles ϕ_1, ϕ_1', ϕ_2 and ϕ_2' are defined in Figure 17.

References

[1] J. B. Keller, "Geometrical Theory of Diffraction," Journal of Optical Society of America, Vol. 52, pp 116-130, 1962.

[2] S. N. Karp and J. B. Keller, "Multiple Diffraction by an Aperture in a Hard Screen," Optica Acta, Vol. 8, pp 61-72, January 1961.

[3] R. G. Kouyoumjian, "The Geometrical Theory of Diffraction and its Applications," in *Numerical and Asymptotic Technique in Electromagnetics*, R. Mittra, ed. New York, Springer Verlag, 1975.

[4] P. H. Pathak, "Techniques for High Frequency Problems," Chapter in *Handbook of Antenna Theory and Design*, eds. Y. T. Lo and S. W. Lee, to be published by ITT-Howard W. Sams and Co., Inc.

[5] R. Mittra and S. W. Lee, *Analytical Techniques in the Theory of Guided Waves*, The Macmillan Company, New York, 1971.

[6] R. G. Kouyoumjian, P. H. Pathak and W. D. Burnside,"A Uniform GTD for the Diffraction by Edges, Vertices and Convex Surfaces," in *Theoretical Methods for Determining the Interaction of Electromagnetic Wave with Structures*, J. K. Skwirzynski, ed., Netherlands, Sijthoff and Noordhoff, 1981.

[7] W. D. Burnside and L. Peters, Jr., "Axial RCS of Finite Cones by the Equivalent Current Concept with Higher Order Diffraction," Radio Science, Vol. 7, No. 10, pp. 943-948, October, 1972.

[8] E. F. Knott and T. B. A. Senior, "Comparison of Three High Frequency Diffraction Techniques," Proceeding of IEEE, Vol. 62, pp. 1468-1474, 1974.

[9] A. Altıntaş, "Electromagnetic Scattering from a Class of Open-Ended Waveguide Discontinuities," Ph. D. Dissertation, The Ohio State University, Department of Electrical Engineering, Columbus, Ohio, Winter 1986.

[10] C. C. Huang, P. H. Pathak, C. Y. Lai and D. L. Moffatt, "Analysis of Electromagnetic Backscatter from an Inlet Cavity Configuration," Final Report 712661-4, October 1982, The Ohio State University ElectroScience Laboratory, Department of Electrical Engineering; prepared under Contract No. F19628-80-C-0056 for the Department of the Air Force, Electronic Systems Command, Hanscom Air Force Base.

[11] J. Pace and R. Mittra, "Generalized Scattering Matrix Analysis of Waveguide Discontinuity Problems," Quasi-Optics, Vol. XIV, pp. 177-197, Polytechnic Institute of Brooklyn Press, New York, 1964.

[12] R. Tiberio, G. Manara, G. Pelosi and R. G. Kouyoumjian, "High-Frequency Diffraction by a Double Wedge," to be published in IEEE AP-S.

[13] P. H. Pathak, C. W. Chuang and M. C. Liang,"Inlet Modeling Studies," Technical Report 717674-1, October 1986, The Ohio State University Electroscience Laboratory, Department of Electrical Engineering;

29

prepared under Contract No. N60530-85-C-0249 for the Department of the Navy, Navy Weapons Center, China Lake, CA 93555.

[14] P. H. Pathak and A. Altıntaş, "An efficient High Frequency Analysis of Modal Reflection and Transmission Coefficients for a Class of Waveguide Discontinuities," to appear in Radio Science.
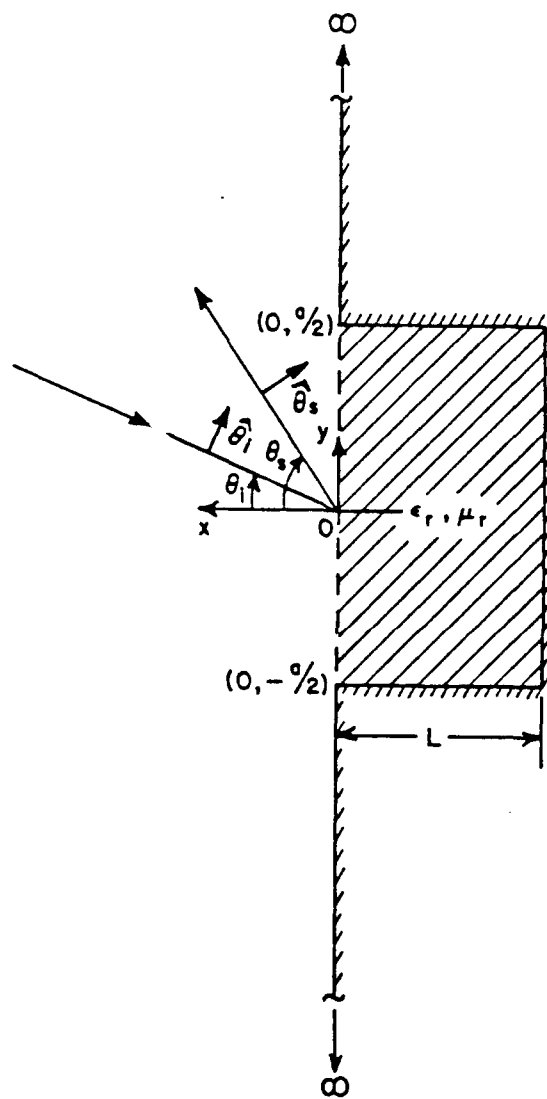
Figure 1: Geometry of the two dimensional cavity with a short end.
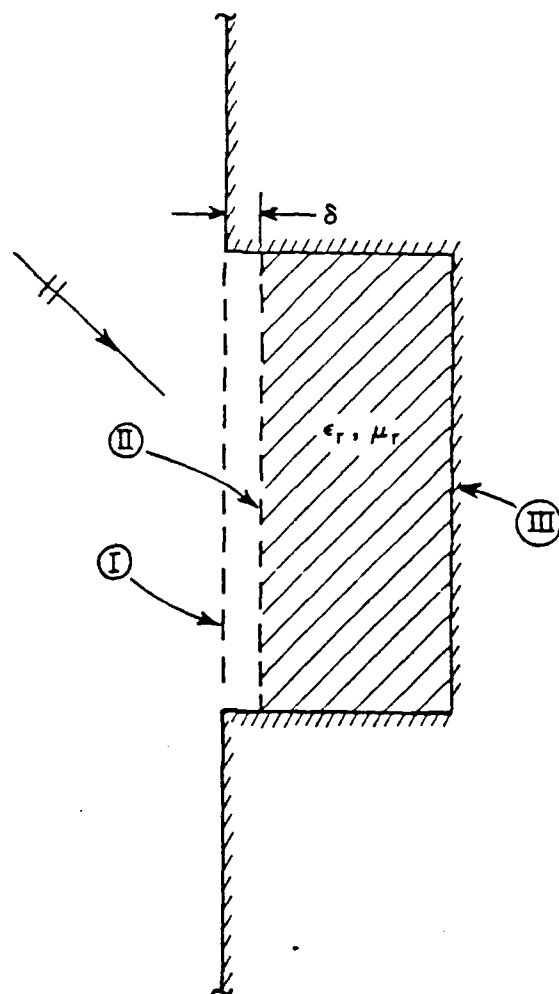
Figure 2: Junctions I, II and III associated with problem in Figure 1. As $\delta \to 0$, the geometry of Figure 2 reduces to that in Figure 1.
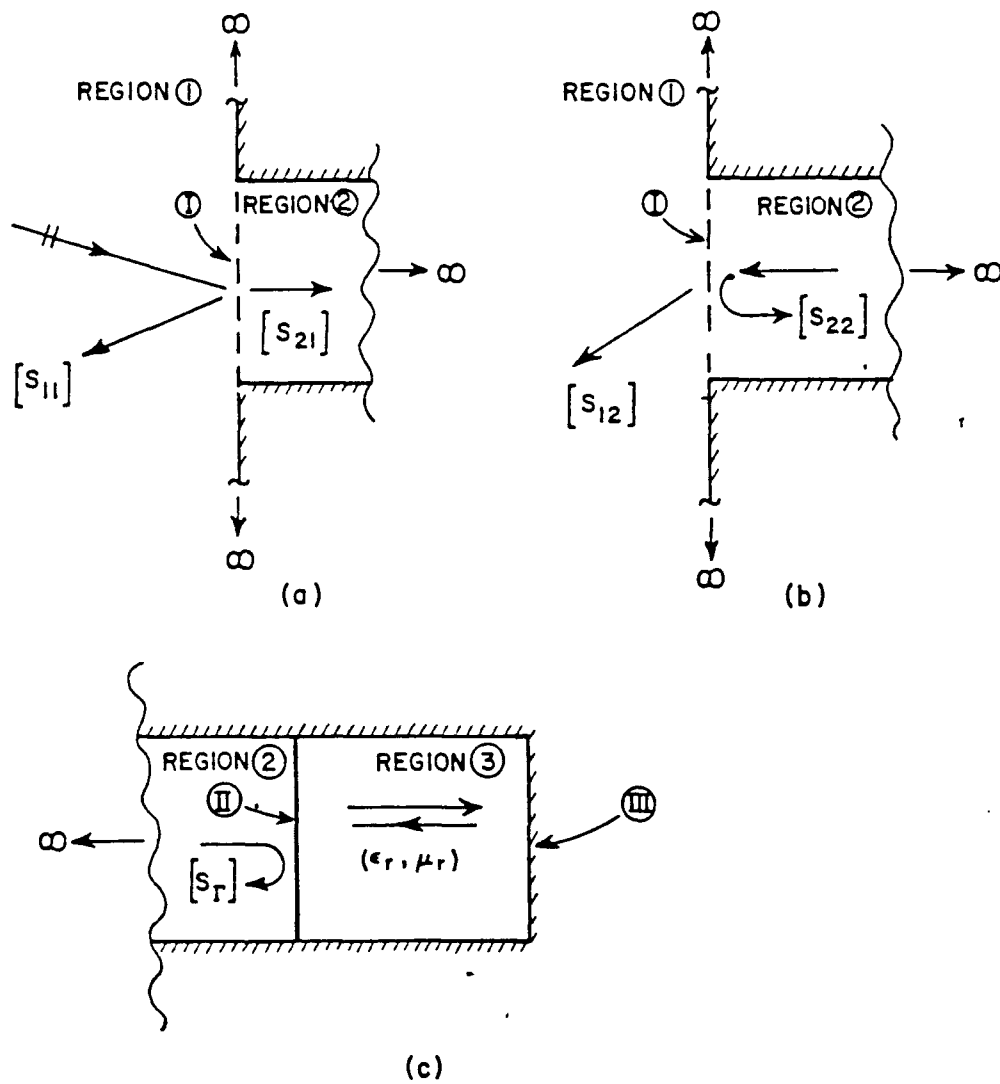
Figure 3: Isolated interactions at junctions I, II and III.

33
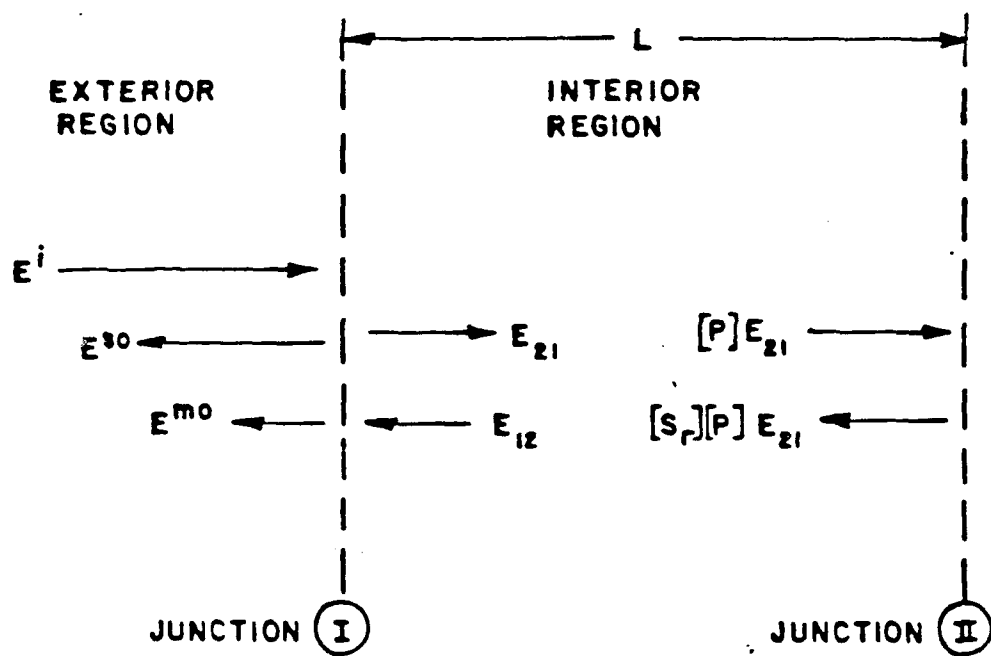
Figure 4: The Interactions of the Multiple Scattering Matrix.

34
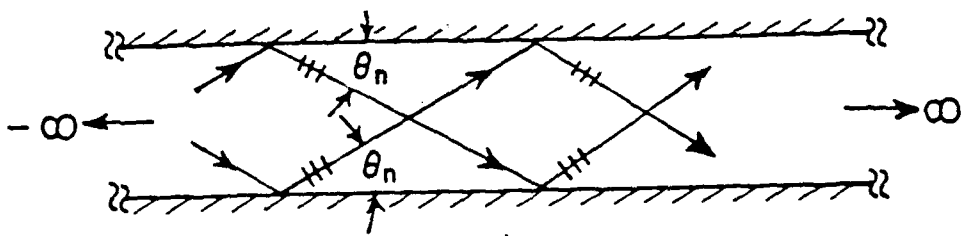
Figure 5: Modal Rays for the Parallel Plate Waveguide
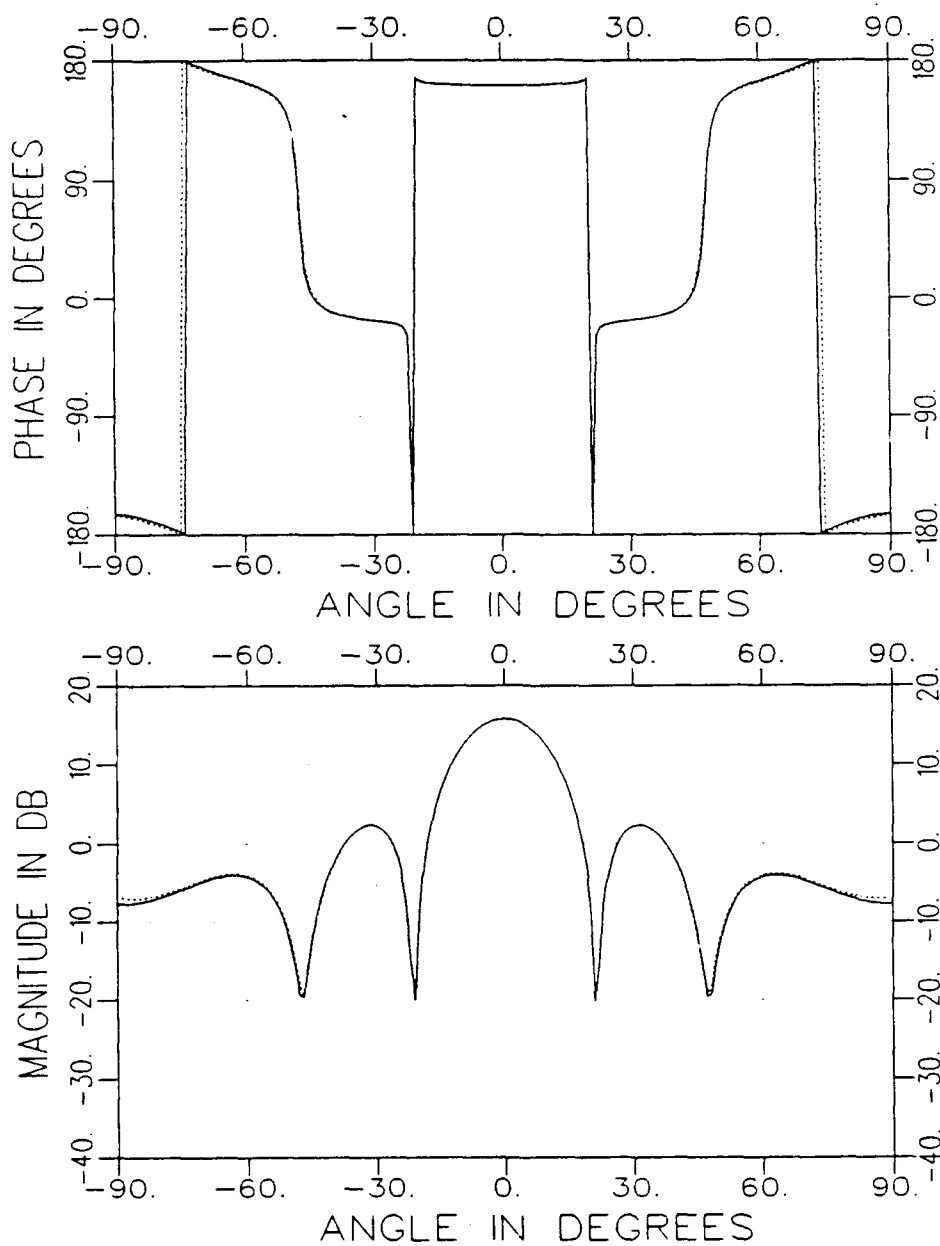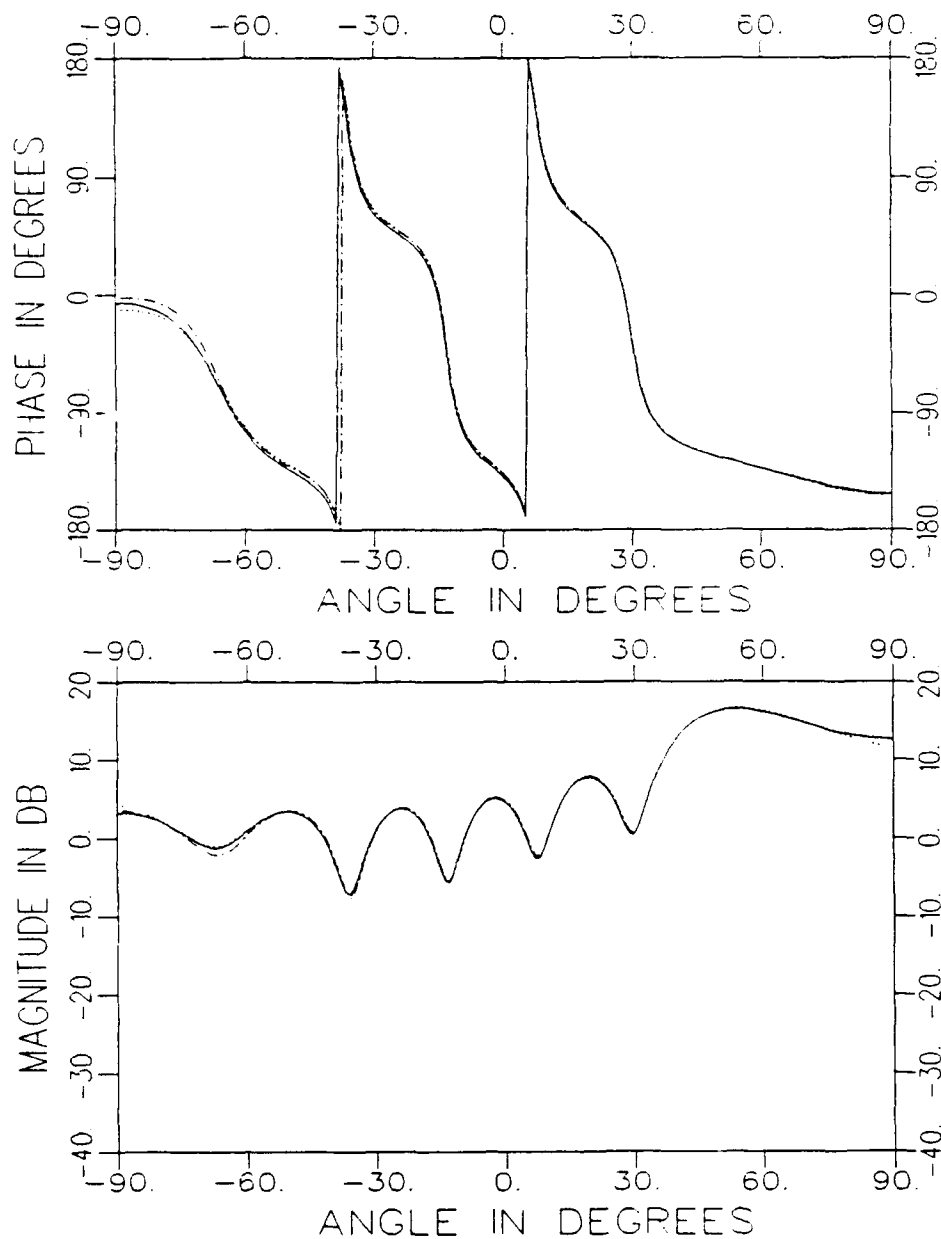
(a) TE$_z$ Case

— MM, - - - AMSM (with Simple Double Diff.),

- · - AMSM (with Single Diff. only) and

- - AMSM(with Modif. TK Double Diff.).

Figure 6: Comparison Between Moment Method and AMSM δ-Approach for the Bistatic Scattering Case with a = 2.8 λ, L = 0.25 λ, ϵ_r = 2.49, μ_r = 1 and θ_i = 0°.
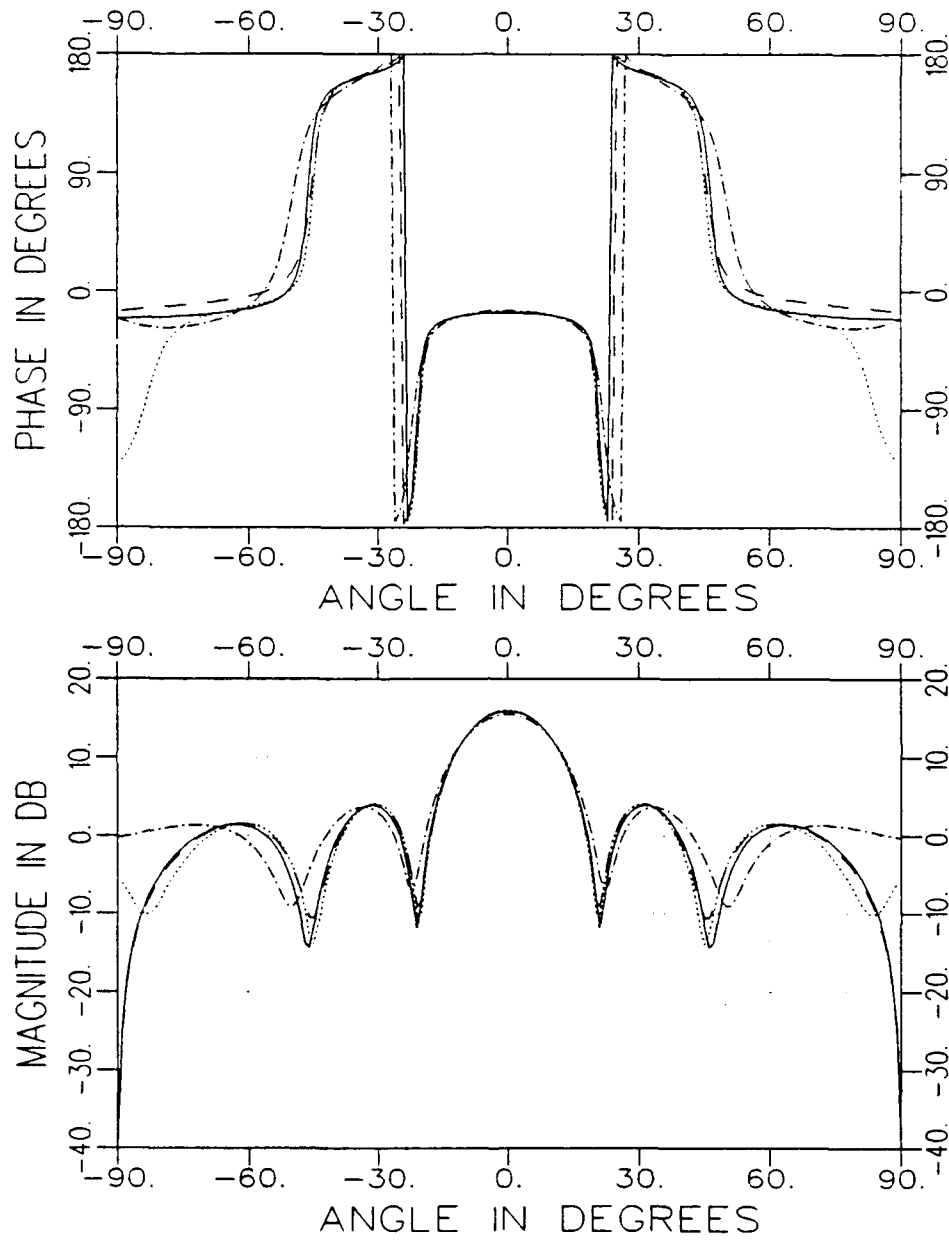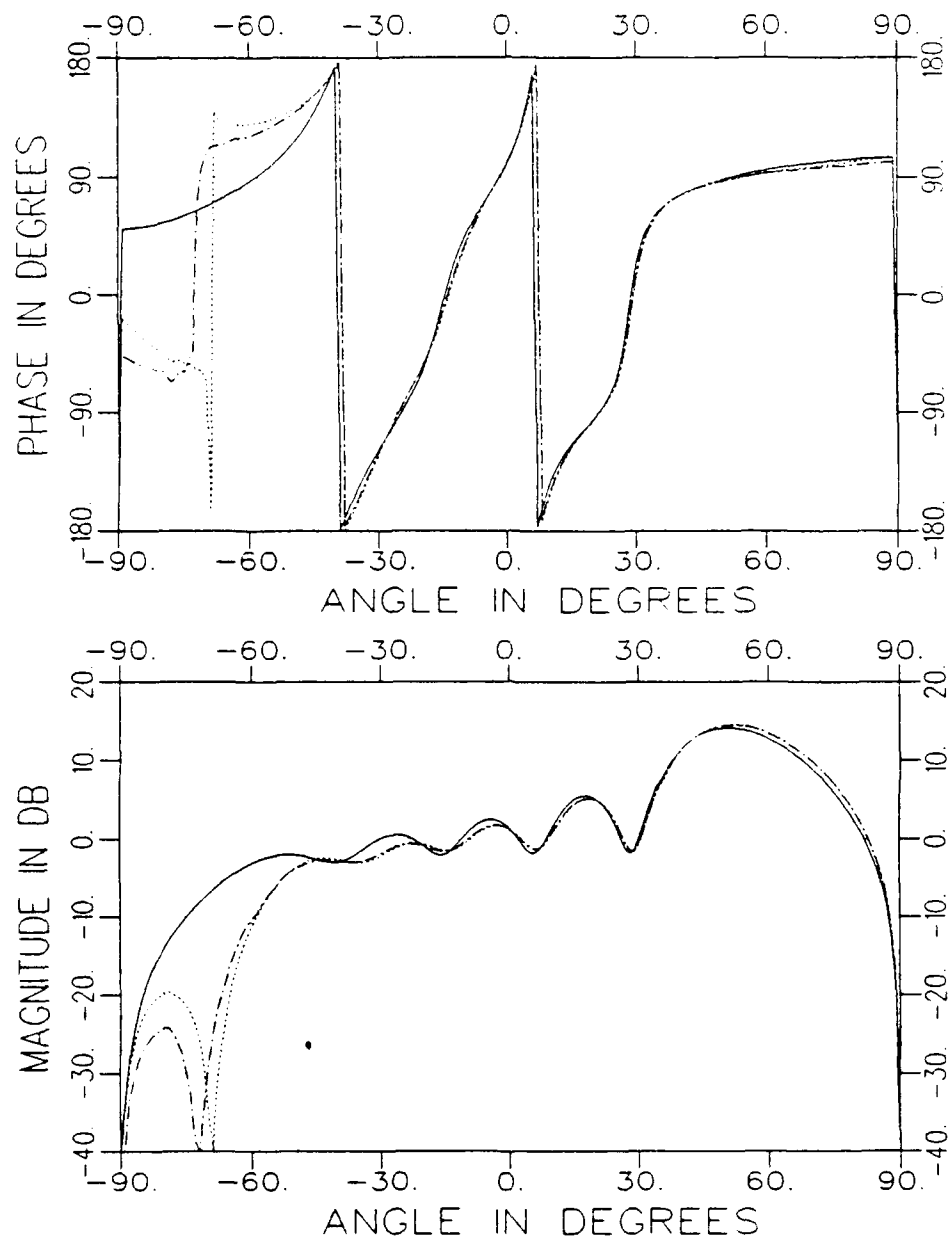
(b) TM$_z$ Case

Figure 6: (Continued)
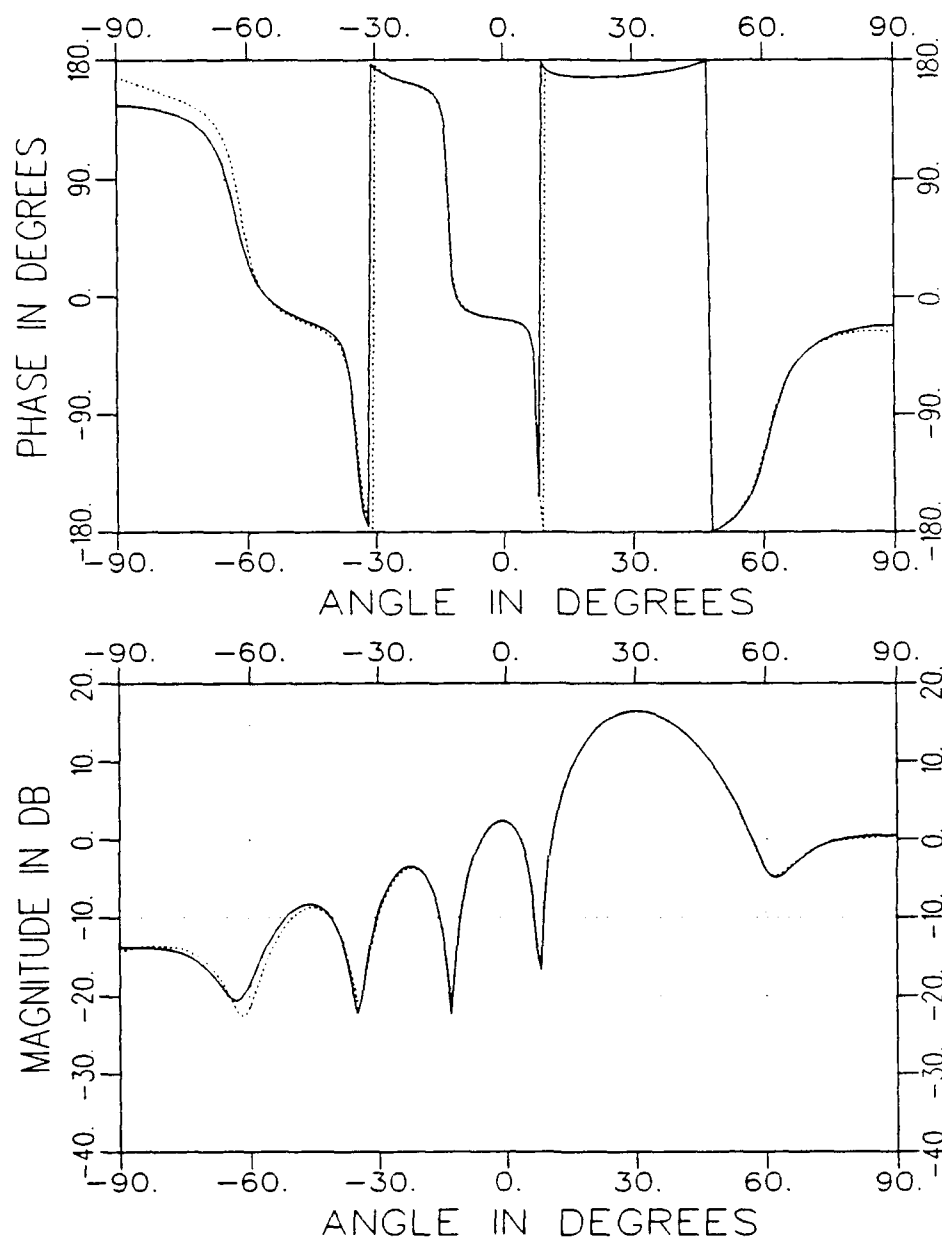
37

(a) TE$_z$ Case

— MM, - - - AMSM (with Simple Double Diff.),

- · · - AMSM (with Single Diff. only) and

- - AMSM (with Modif. TK double Diff.).

Figure 7: Comparison Between Moment Method and AMSM δ-Approach for the Bistatic Scattering Case with a = 2.8 λ, L = 0.25 λ, ϵ_r = 2.49, μ_r = 1 and θ_i = -30°.

38
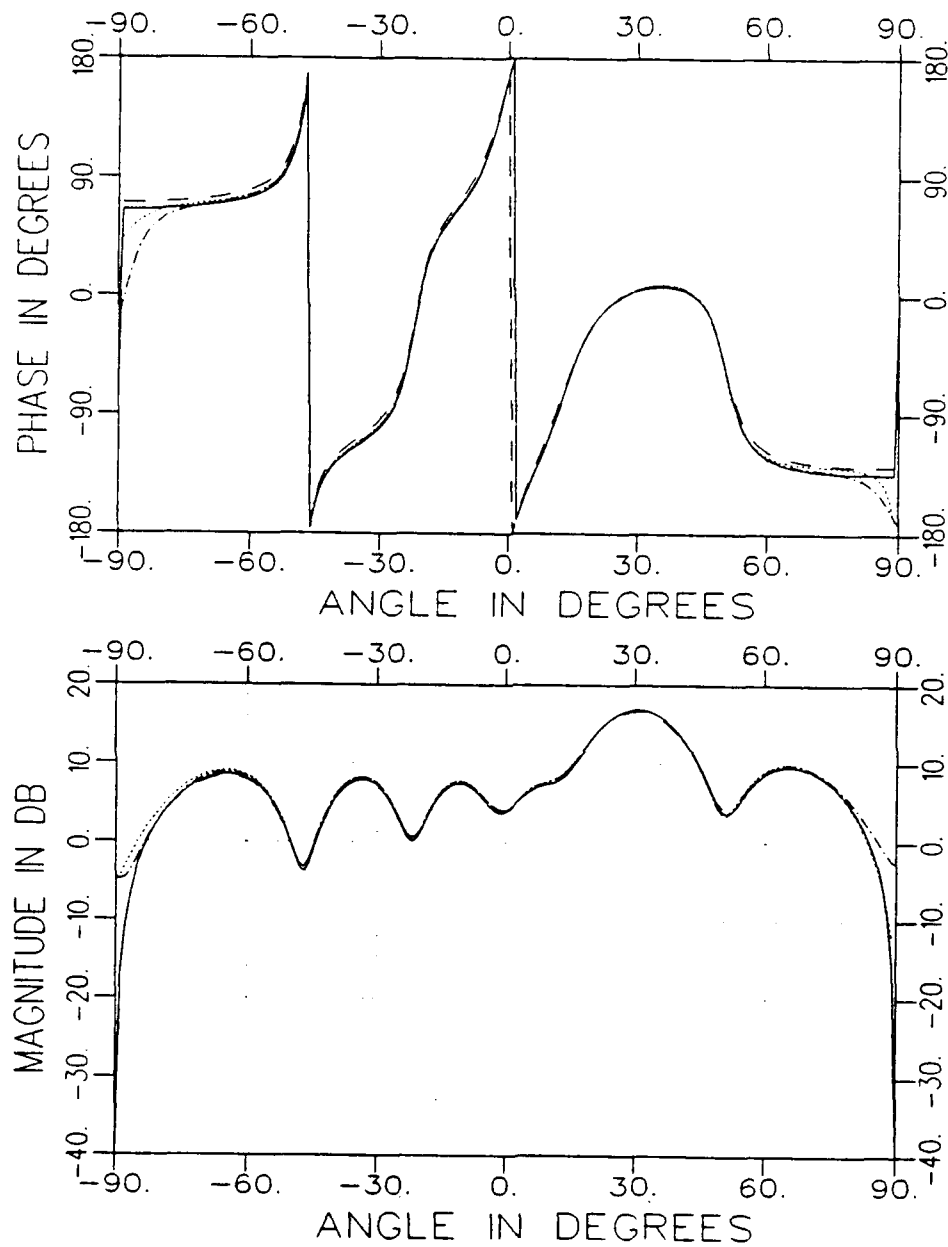
(b) TM$_z$ Case

Figure 7: (Continued)

39
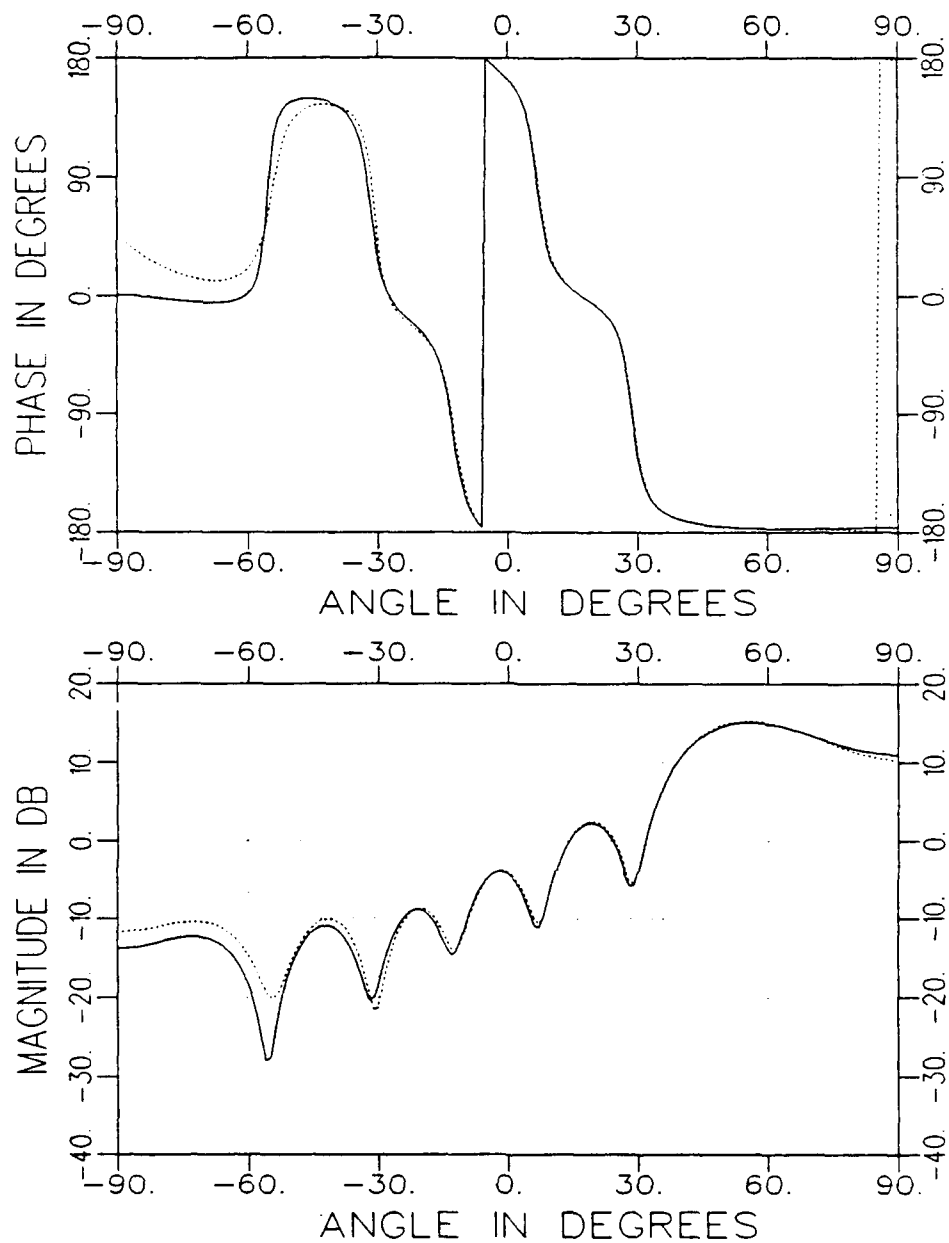
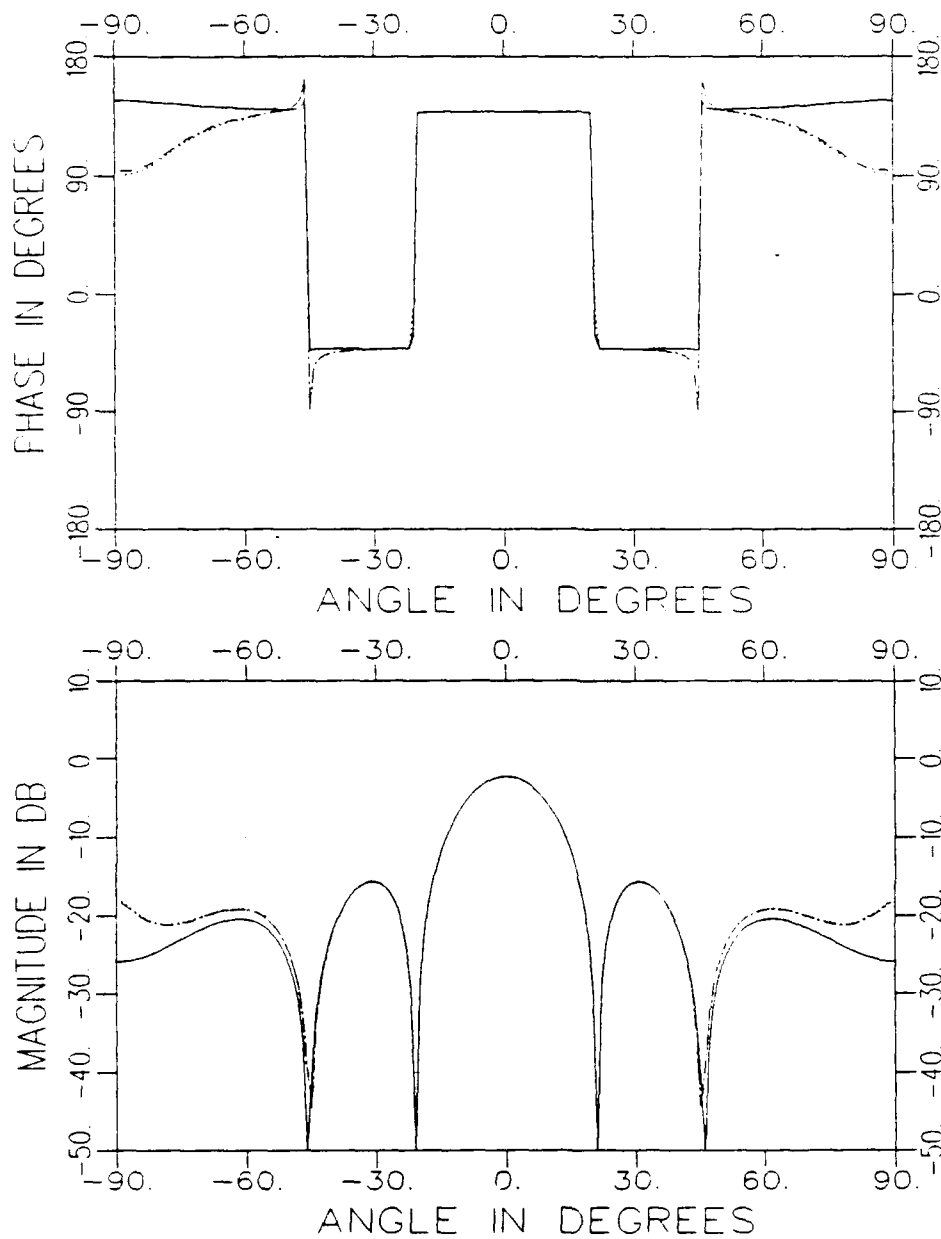(a) TE$_z$ Case

— MM, - - - AMSM (with Simple Double Diff.) and

- · - AMSM (with Single Diff. only).

Figure 8: Comparison Between Moment Method and AMSM δ-Approach for the Bistatic Scattering Case with a = 2.8 λ, L = 0.25 λ, ϵ_r = 2.49, μ_r = 1 and θ_i = -60°.

40
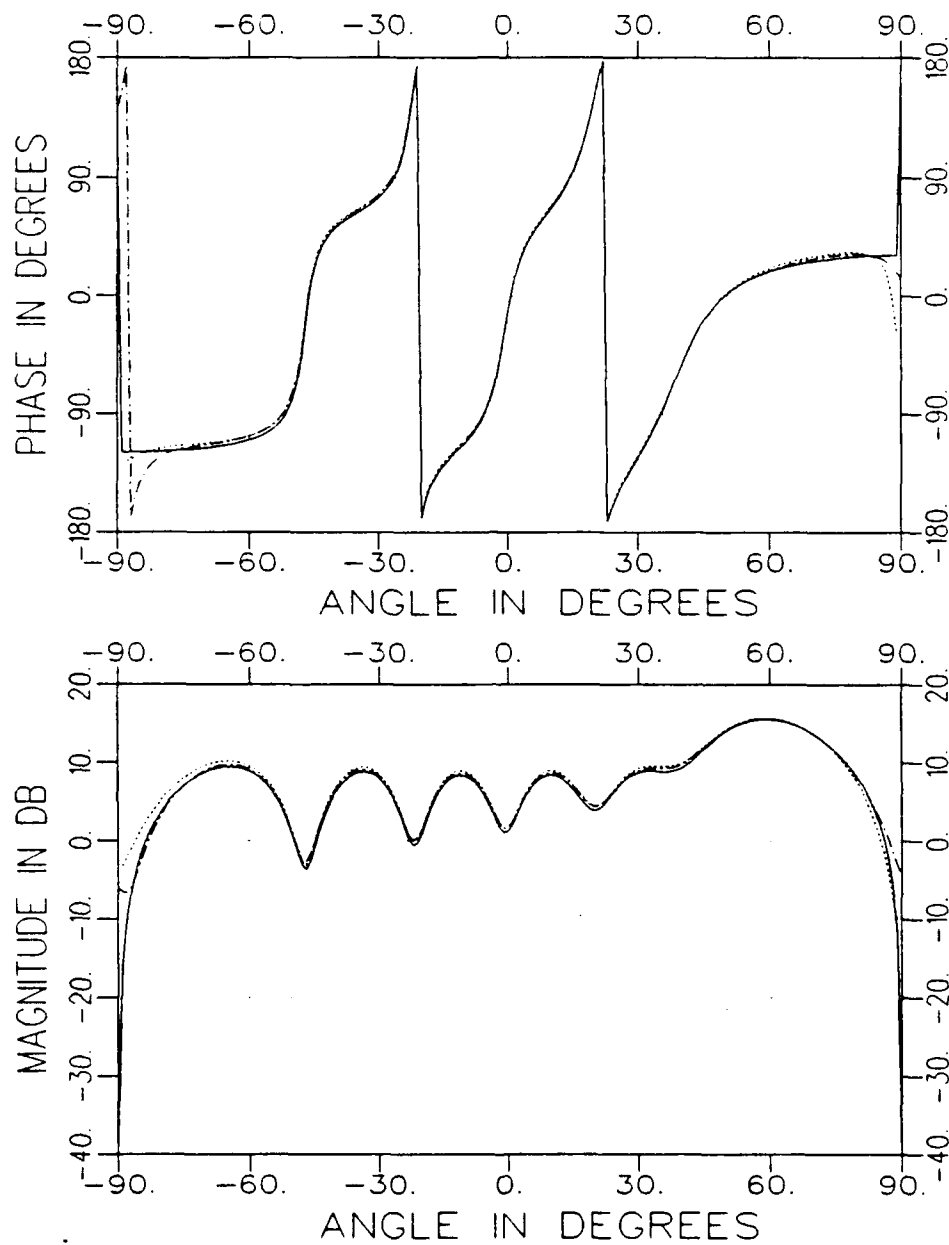
(b) TM$_z$ Case

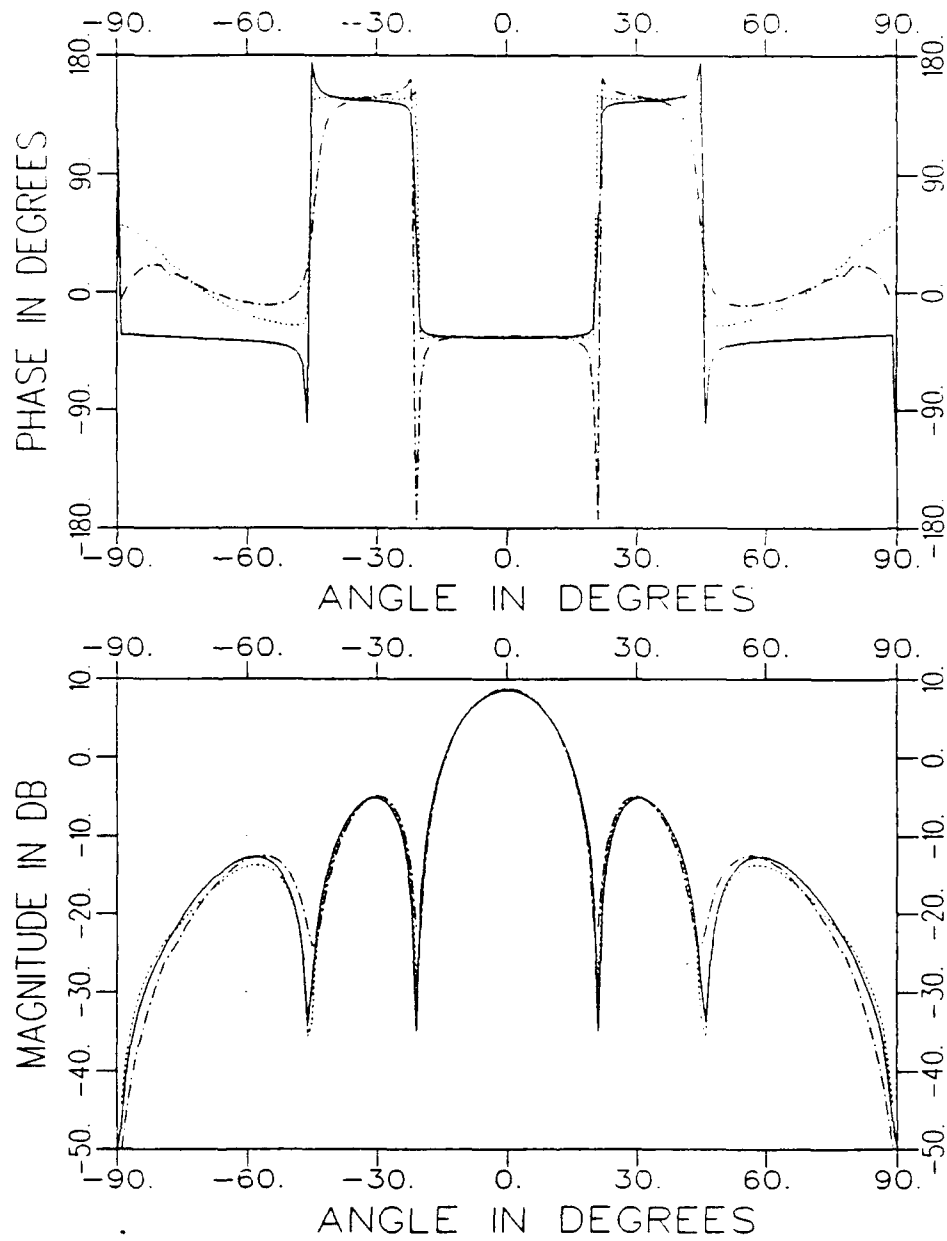Figure 8: (Continued)

41
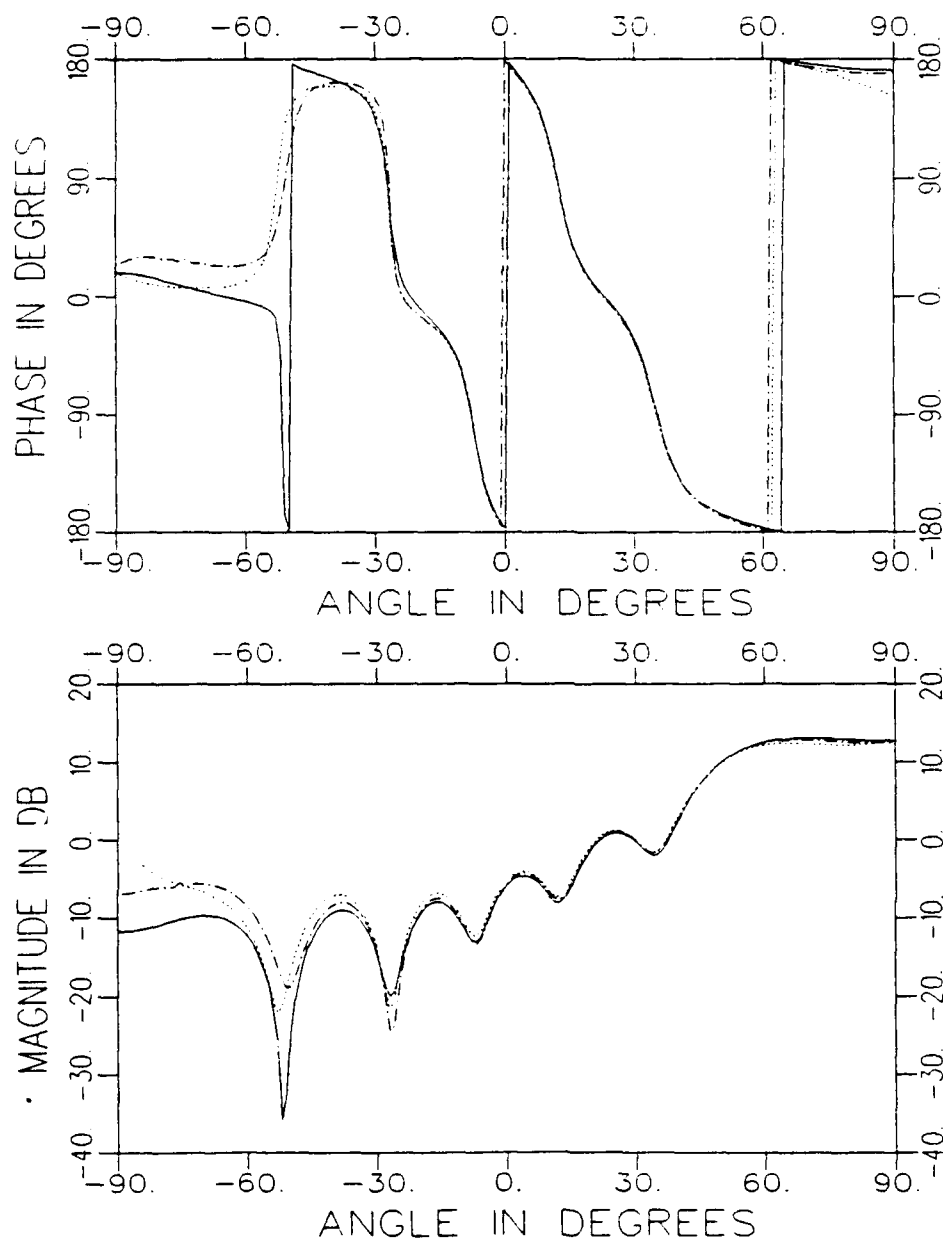
(a) TE$_z$ Case

— MM, - - - AMSM (with Modif. Simple Double Diff.) and

- · - AMSM (with Modif. TK Double Diff.).

Figure 9: Comparison Between Moment Method and AMSM δ-Approach for the Bistatic Scattering Case with a = 2.8 λ, L = 0.25 λ, ϵ_r = 2.49, μ_r = 1 and θ_i = -75°.   42
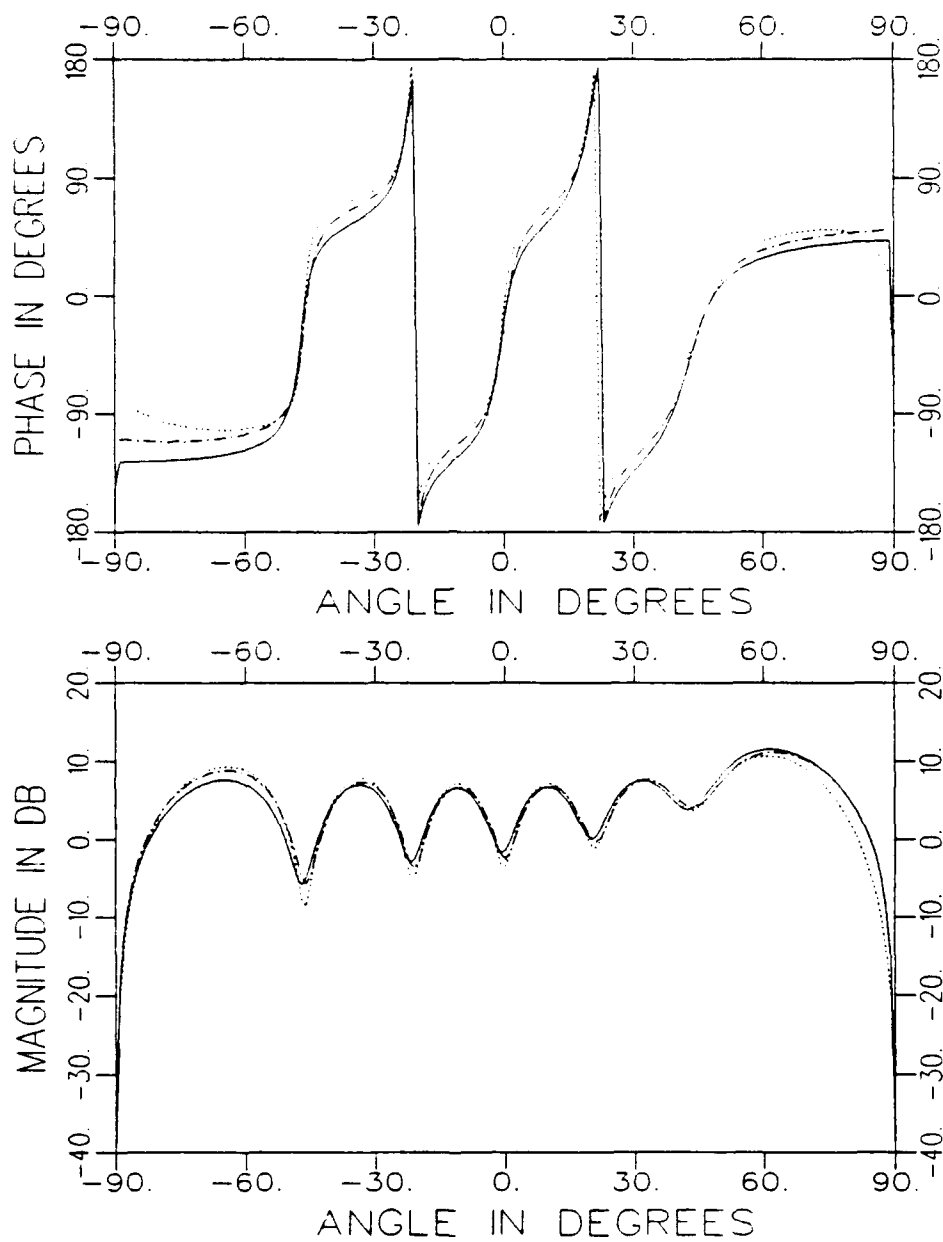
(b) TM$_z$ Case

Figure 9: (Continued)

43
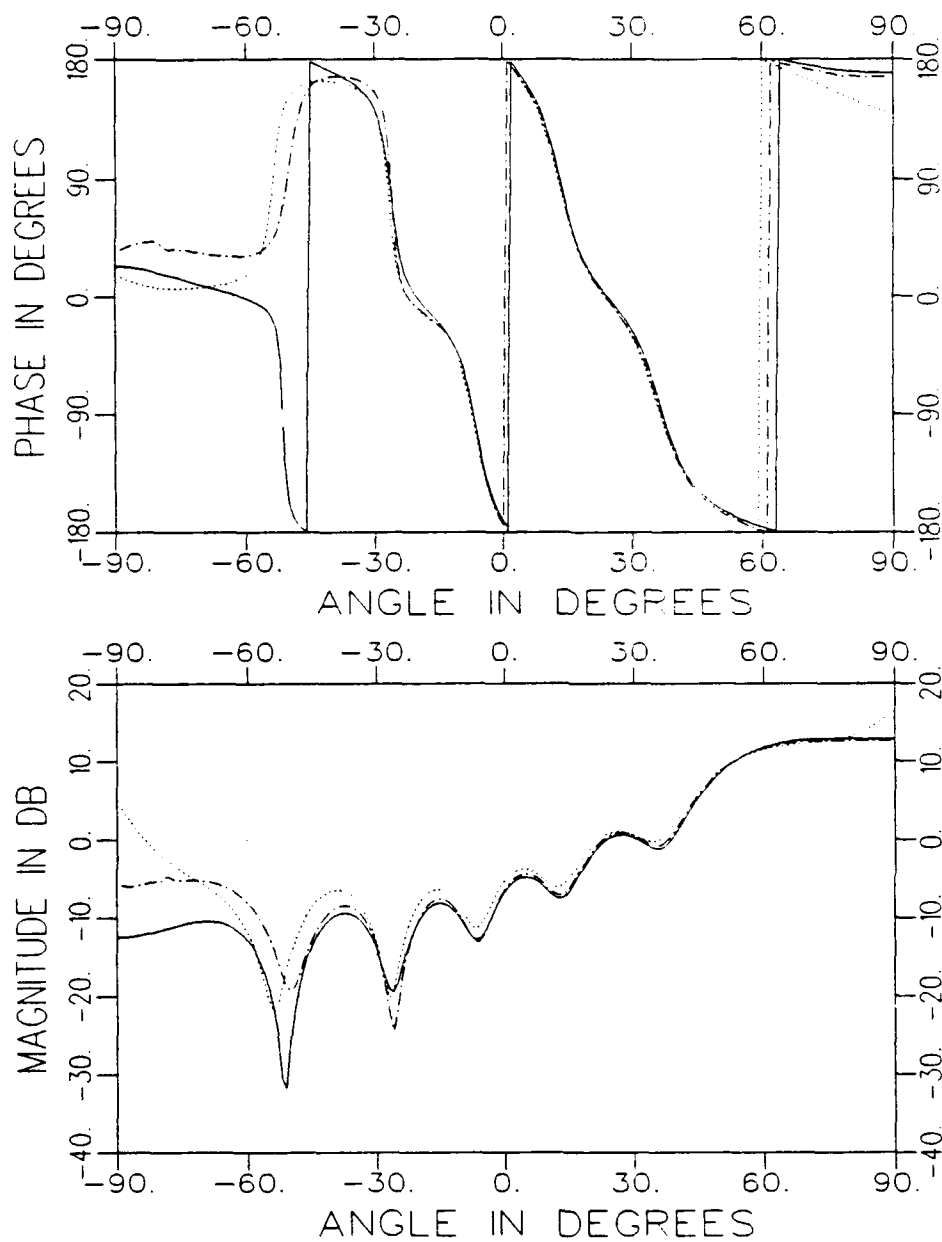
(a) TE$_z$ Case

— MM, - - - AMSM (with Modif. Simple Double Diff.)

and - · - AMSM (with Modif. TK Double Diff.).

Figure 10: Comparison Between Moment Method and AMSM δ-Approach for the Bistatic Scattering Case with a = 2.8 λ, L = 0.25 λ, ϵ_r = 2.49, μ_r = 1 and θ_i = -80°.   44
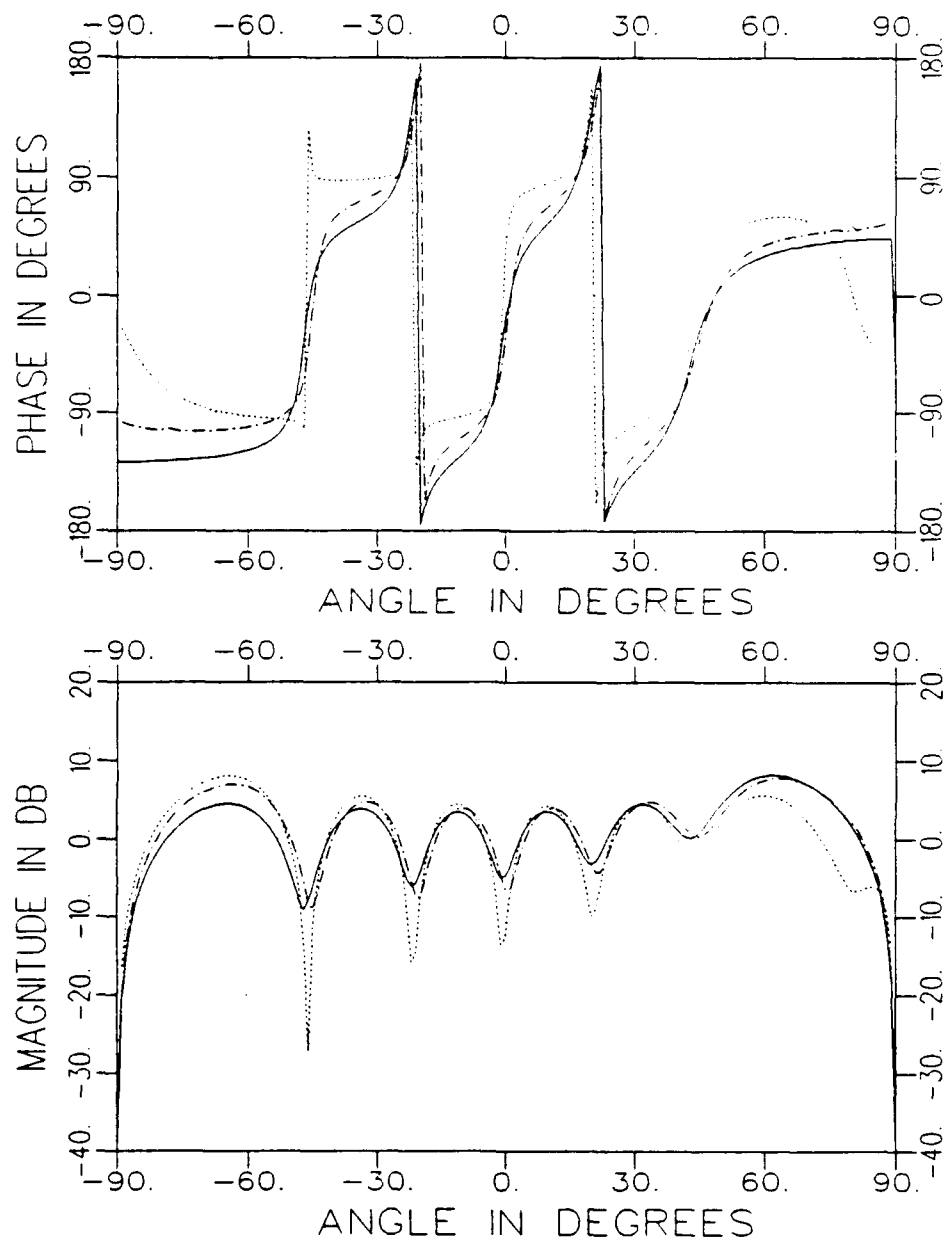
(b) TM$_z$ Case

Figure 10: (Continued)

45

(a) TE$_z$ Case

— MM, - - - AMSM (with Modif. Simple Double Diff.)

- - - AMSM (with Modif. TK Double Diff.)

Figure 11: Comparison Between Moment Method and AMSM for a very shallow rectangular cavity with L = 0.15 λ a = 2.8 λ. The Calculation is for the Bistatic Scattering Case with μ_r = 1, ϵ_r = 2.49 and θ_i = -60°.

46

(b) TM$_z$ Case

Figure 11: (Continued)

47

(a) TE$_z$ Case with $\epsilon_r = 60$

— MM, - - - AMSM (with Modif. Simple Double Diff.) and

- · - AMSM (with Modif. TK Double Diff.)

Figure 12: Comparison Between Moment Method and AMSM for a high dielectric loading. The Calculation is for the Bistatic Scattering Case with $a = 2.8\ \lambda$, L $= 0.25\ \lambda$, $\mu_r = 1$ and $\theta_i = 0°$.
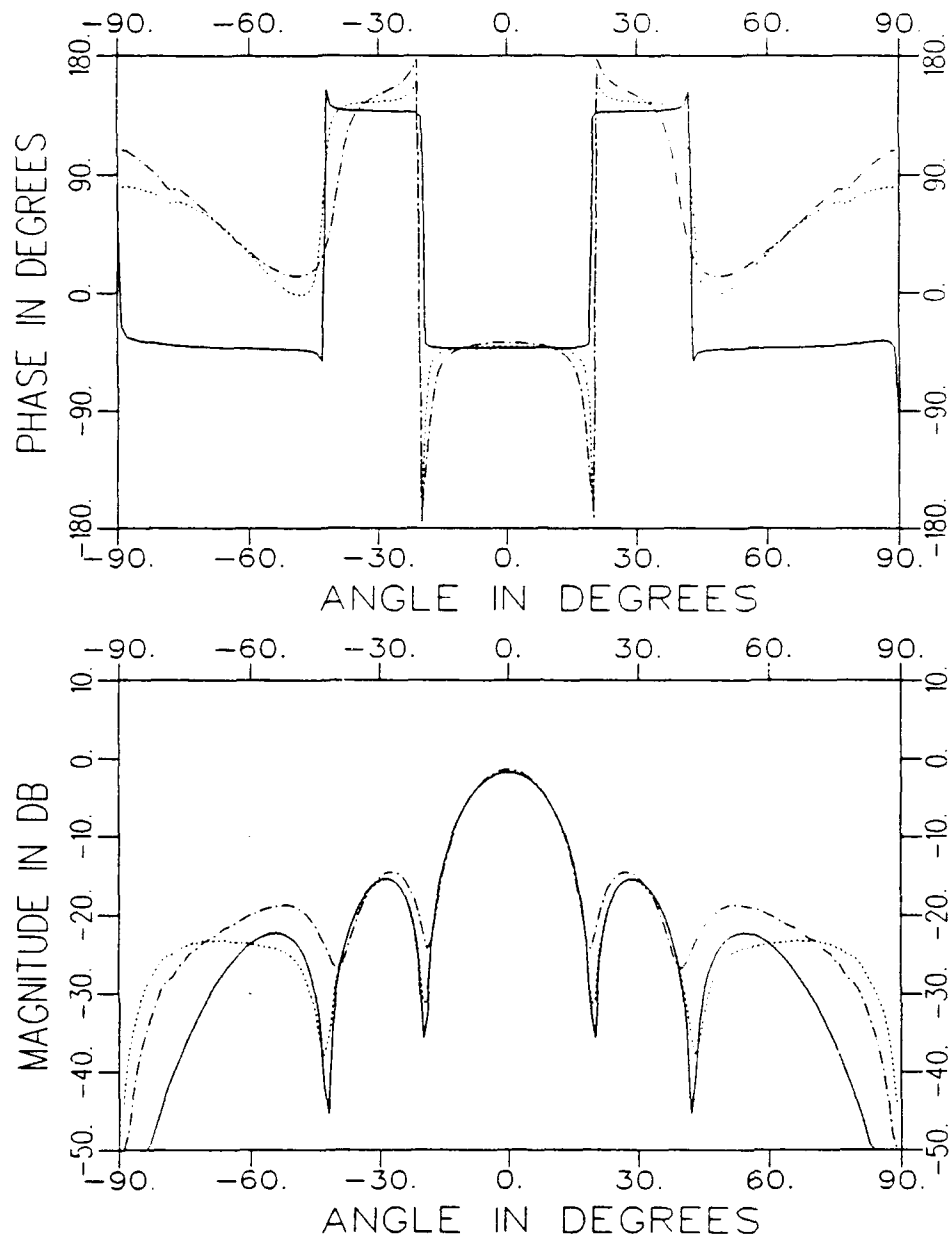
(b) TM$_z$ Case with $\epsilon_r = 60$

Figure 12: (Continued)

49

(c) TM_z Case with $\epsilon_r = 30$

Figure 12: (Continued)

50
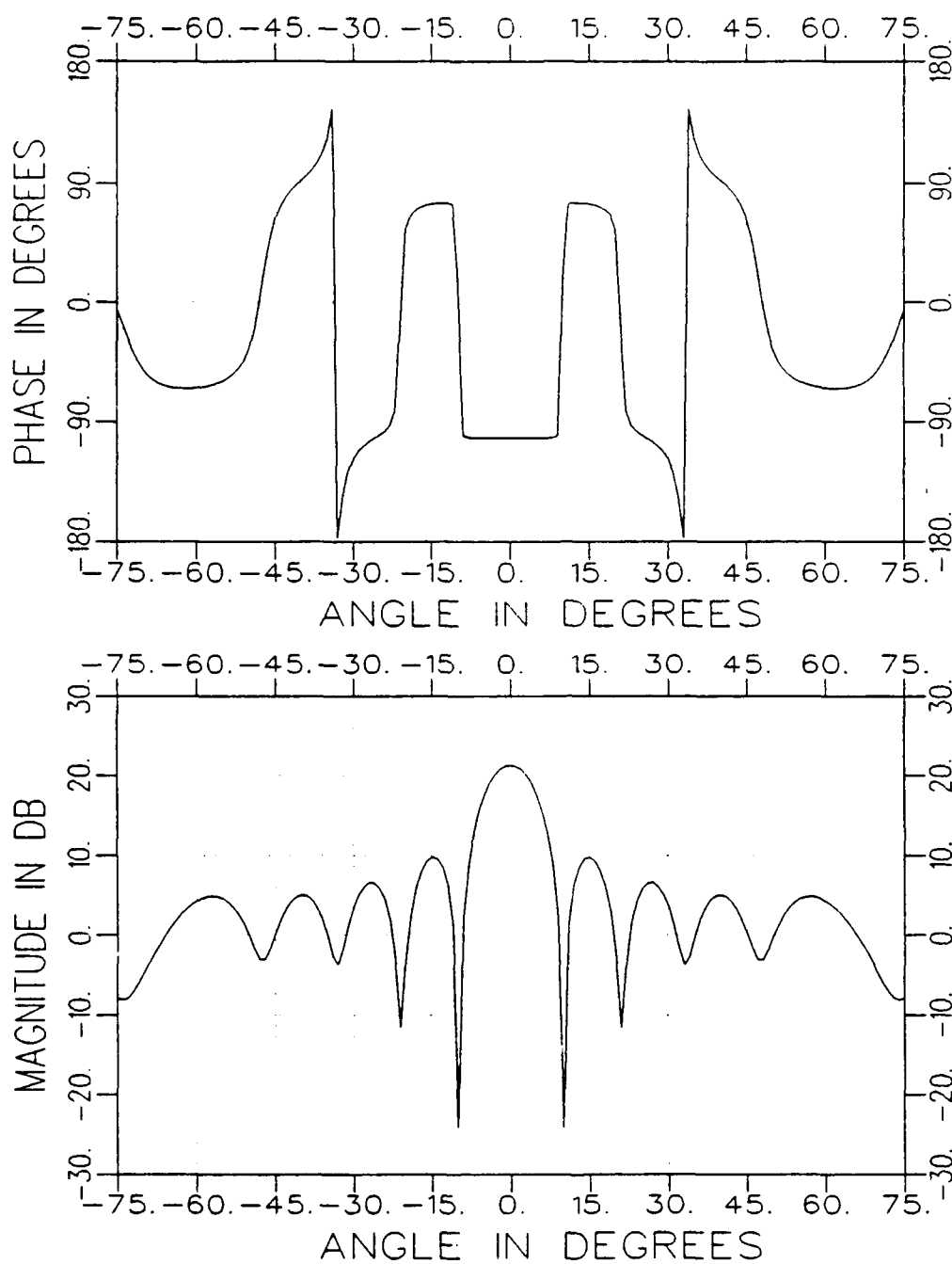
(a) TE$_z$ Case

Figure 13: The AMSM δ-Approach Calculation for the Backscatter with a = 2.8 λ, L = 0.75 λ, ϵ_r = 2.49, and μ_r = 1.
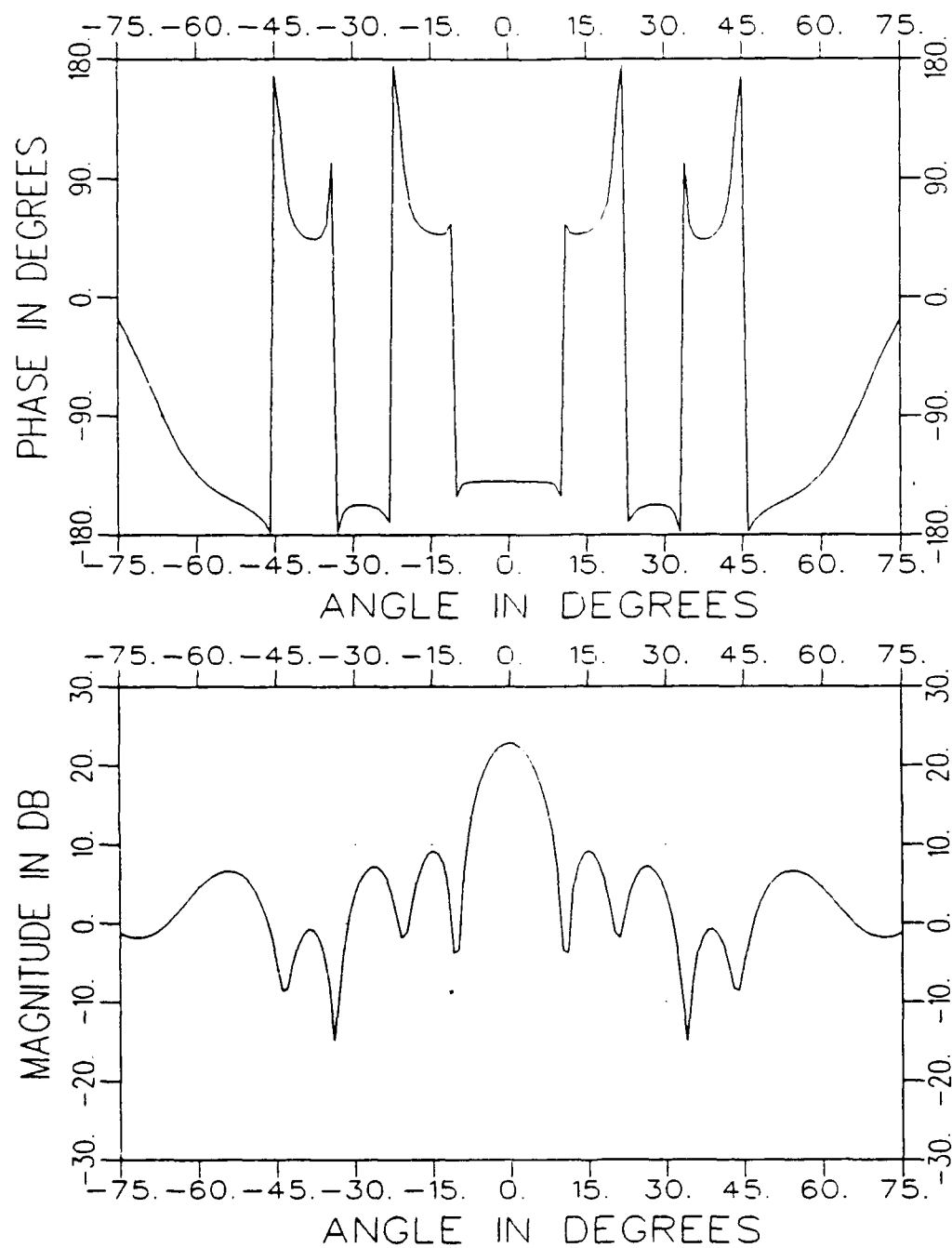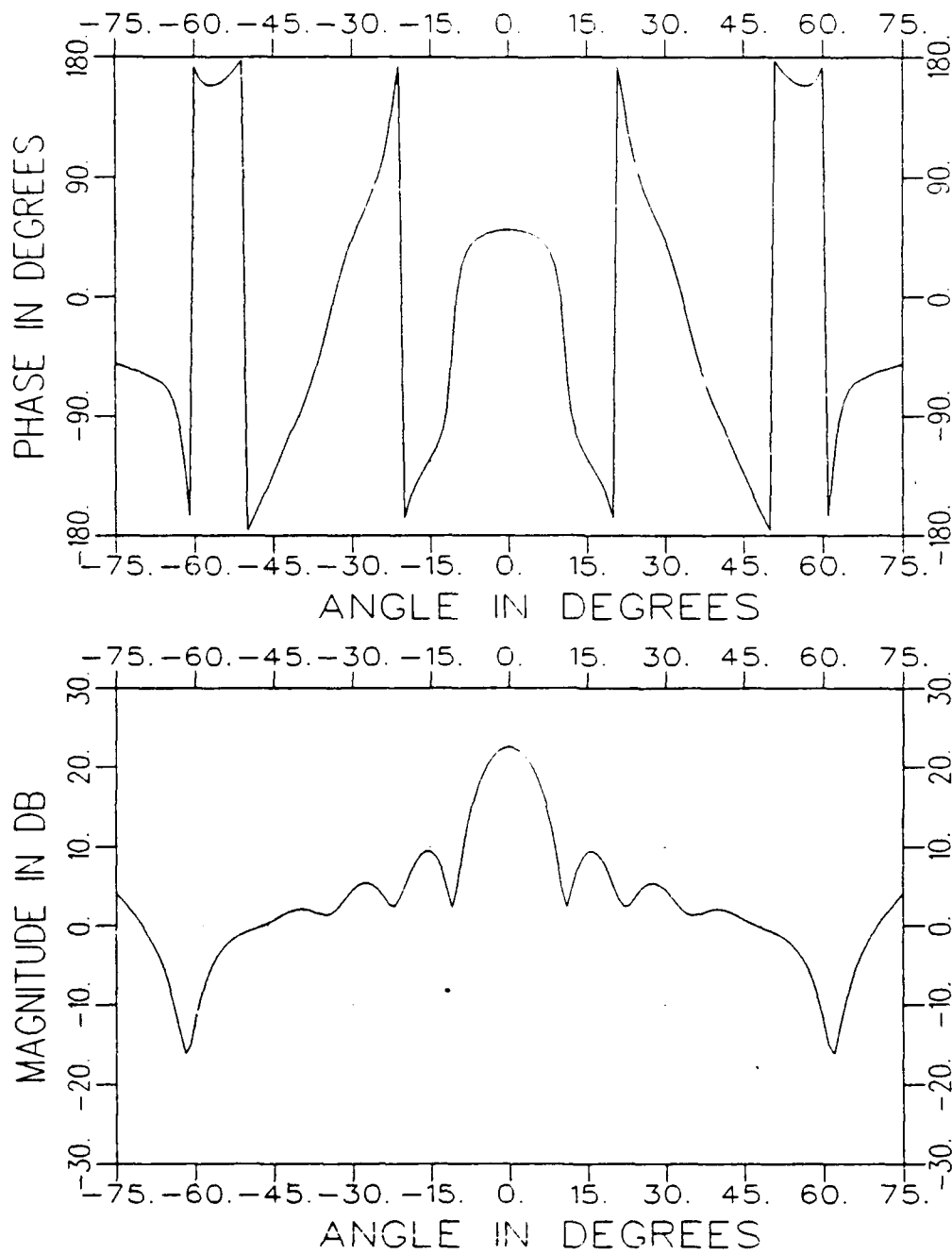
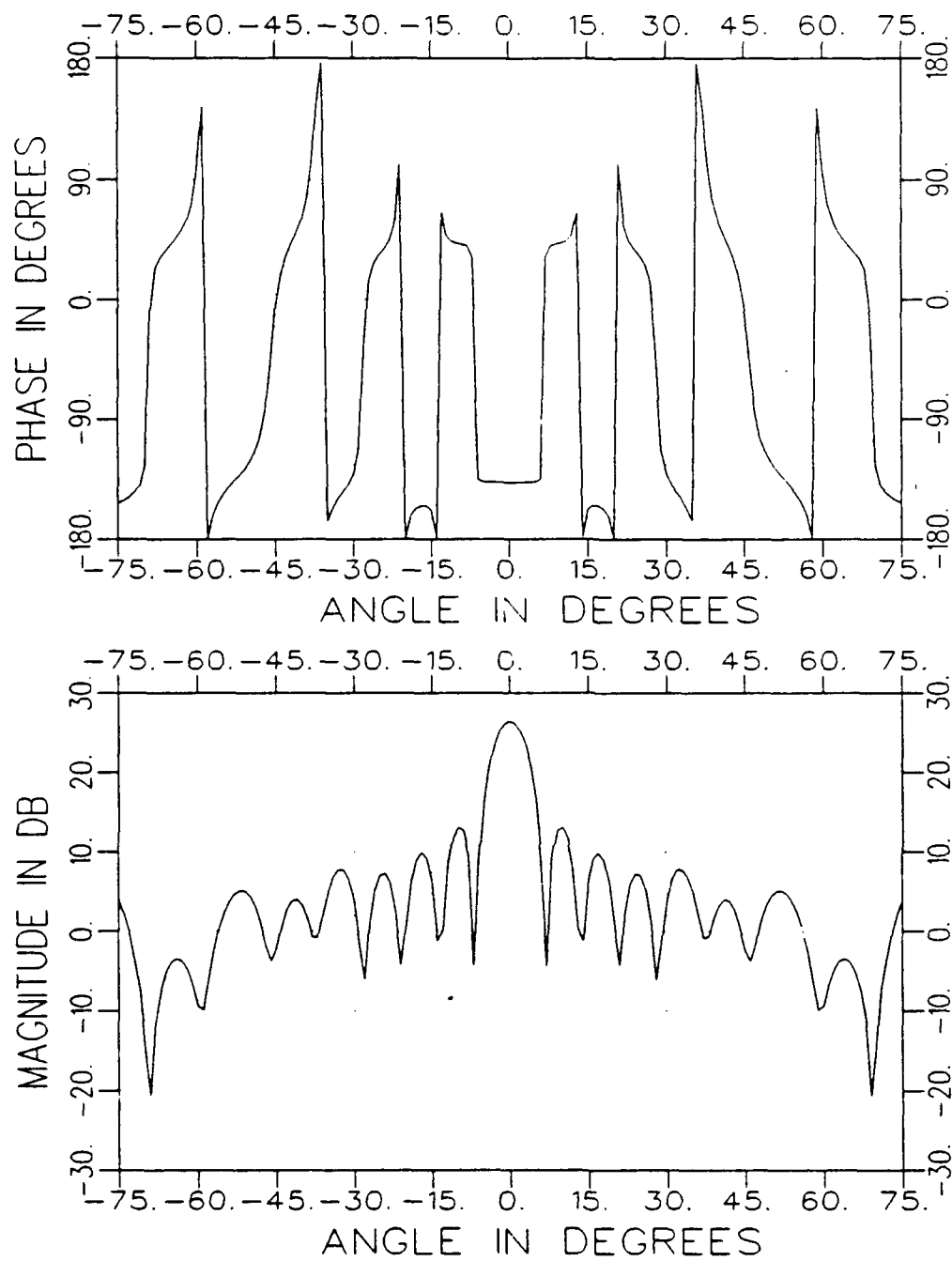51
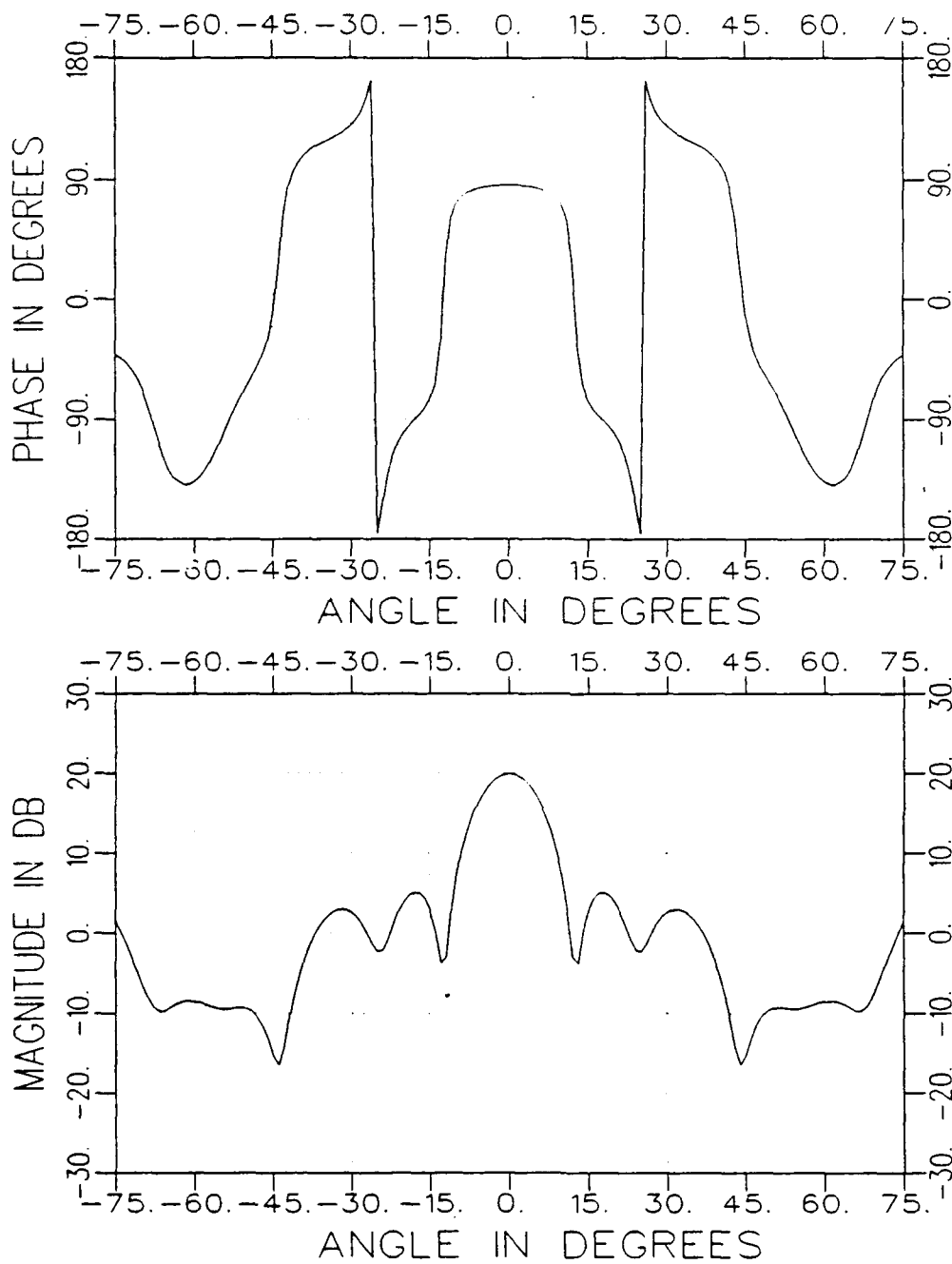
(b) TM$_z$ Case

Figure 13: (Continued)

52
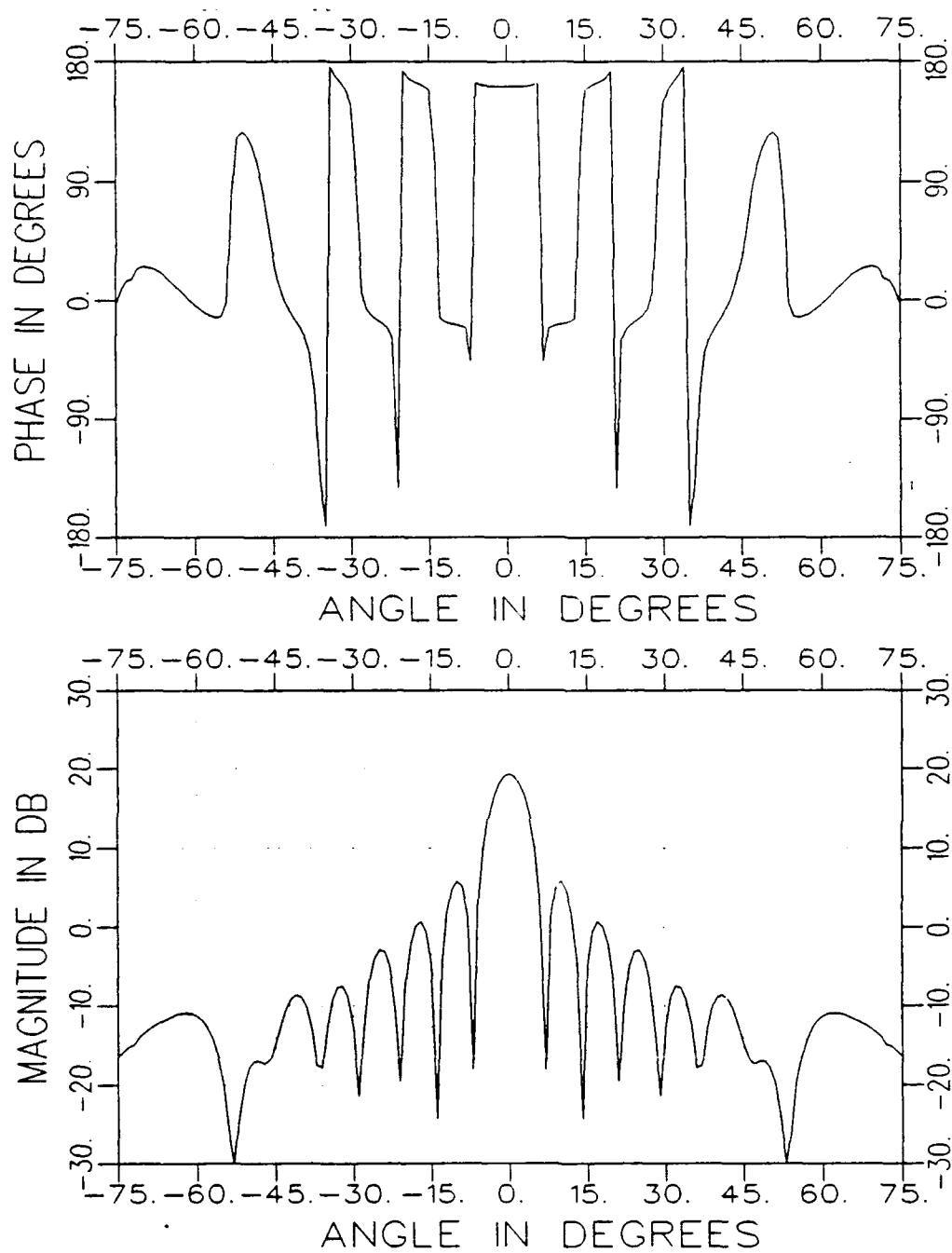
(a) TE$_z$ Case

Figure 14: The AMSM δ-Approach Calculation for the Backscatter with a = 4.2 λ, L = 0.25 λ, ϵ_r = 2.49, and μ_r = 1.

53
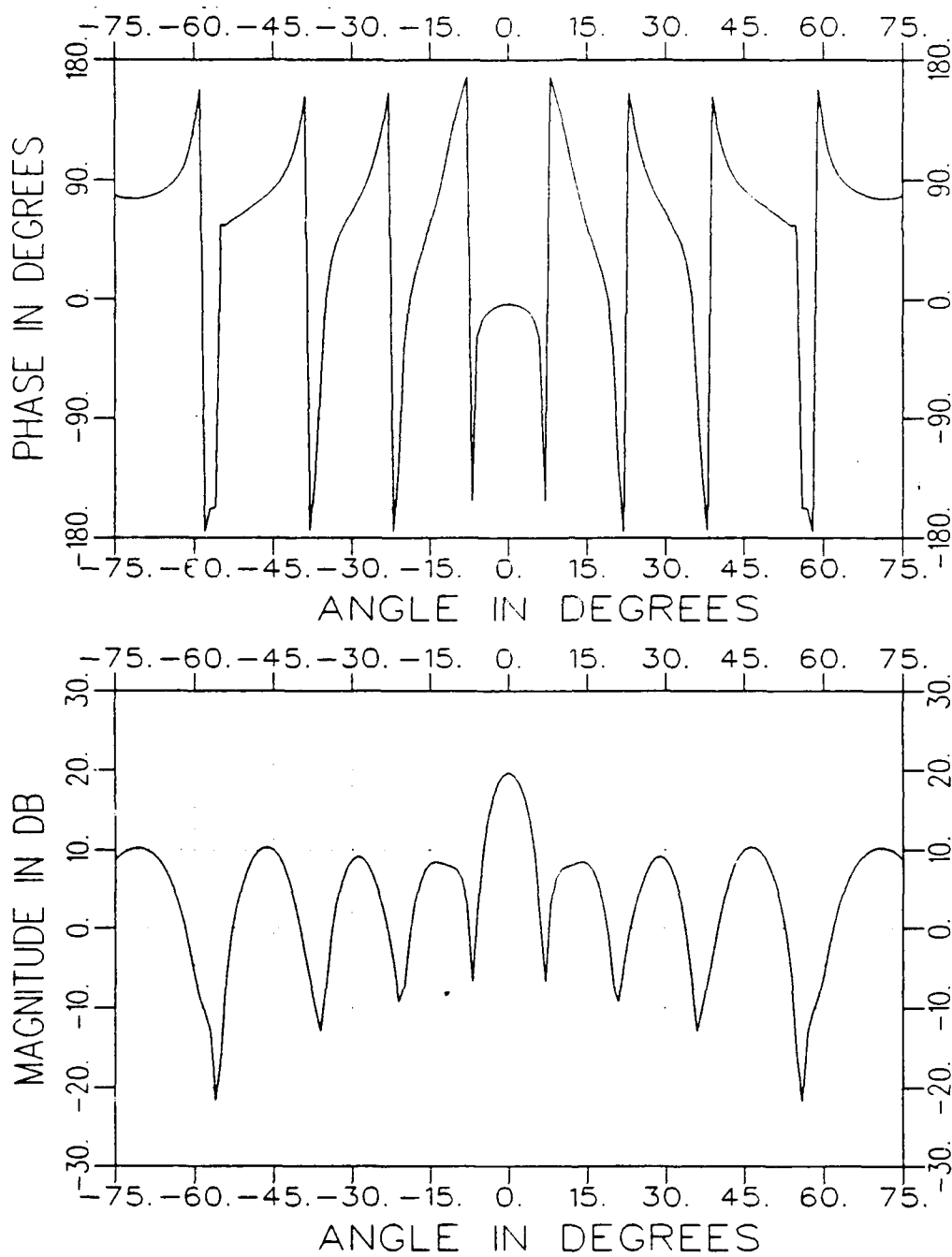
(b) TM$_z$ Case

Figure 14: (Continued)

54

(a) TE_z Case

Figure 15: The AMSM δ-Approach Calculation for the Backscatter with a = 2.8 λ, L = 0.25 λ, ϵ_r = 9., and μ_r = 1.
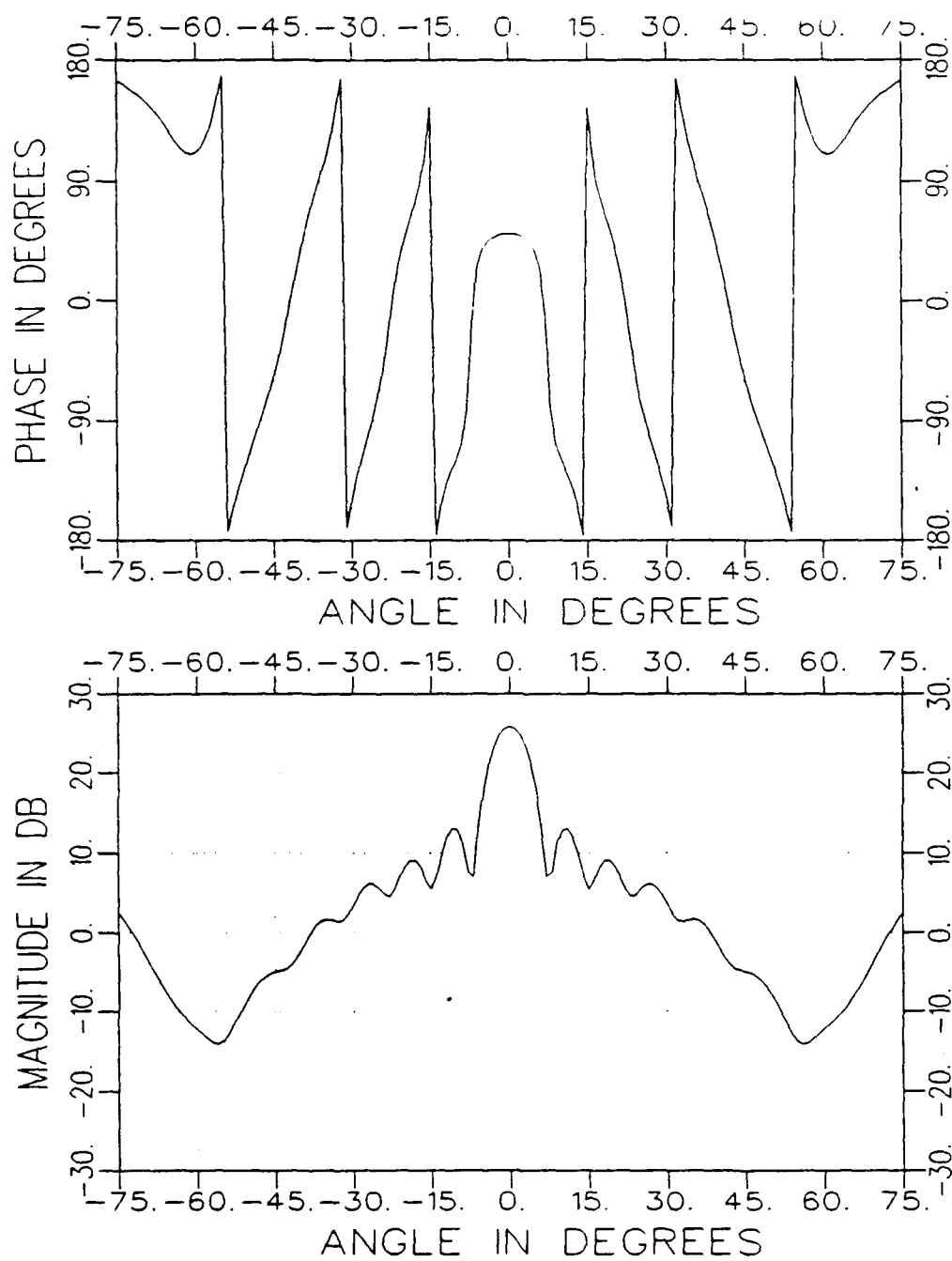
55

(b) TM$_z$ Case

Figure 15: (Continued)

56

(a) TE$_z$ Case

Figure 16: The AMSM δ-Approach Calculation for the Backscatter with a = 4.2 λ, L = 0.75 λ, ϵ_r = 9., and μ_r = 1.

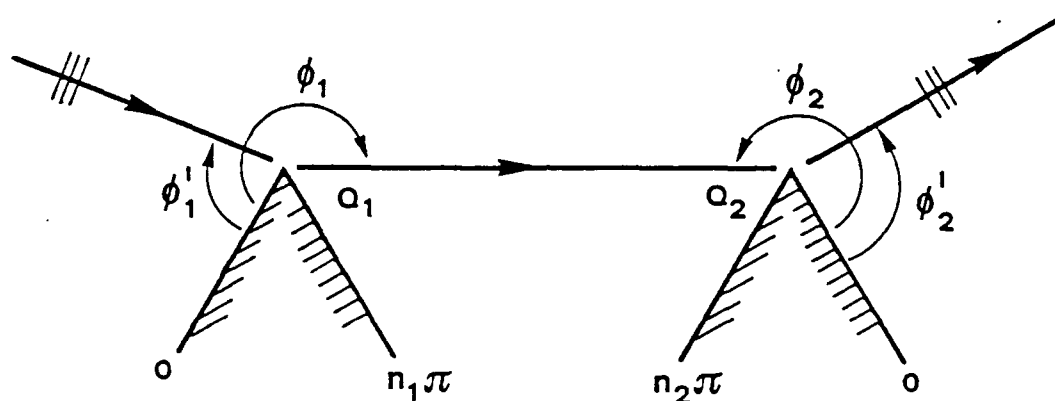(b) TM$_z$ Case

Figure 16: (Continued)

58

Figure 17: The Geometry for the Doubly Diffracted Field Between Two
Edges